Grumman EXPERIMENTAL STUDY OF HIGH-SPEED HYDROFOILS
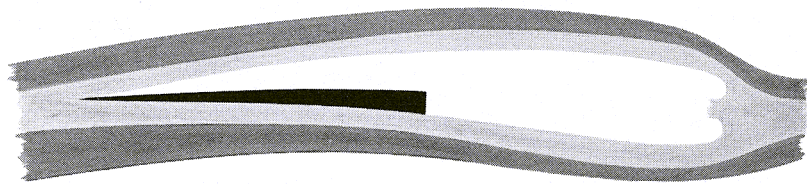
REPORT

NO. XAR-A-45   DATE AUG. 26, 1963

EXPERIMENTAL STUDY OF

HIGH SPEED HYDROFOILS

VOLUME III

CODE 26512

H. R. Wright
PREPARED BY:

T. B. Street
CHECKED BY:

S. C. Wennagel
APPROVED BY:

J. J. Waaland

REVISIONS

DATE	REV BY	REVISIONS & ADDED PAGES	REMARKS

ACKNOWLEDGEMENT

TABLE OF CONTENTS

SUMMARY

This test program was conducted to measure the hydrodynamic characteristics of a series of supercavitating and transcavitating hydrofoil models with various planforms and sections to provide a design procedure to predict hydrodynamic characteristics for this type hydrofoil. Twenty hydrofoil models were tested in the Grumman Whirling Tank at three depths and at a sufficient number of speeds and angles of attack to fully define their hydrodynamic characteristics. Lift, drag, pitching moment, and strut base pressure were measured for all models, and cavity pressure and foil base pressure were measured for the supercavitating models.

Classic supercavitating hydrofoil theory is shown to predict test results with an accuracy adequate for design if a modified value for the cross-flow lift coefficient is accepted.

INTRODUCTION

The work under this contract consisted of testing twenty supercavitating and transcavitating hydrofoil models in the Grumman Whirling Tank at three depths and at a sufficient number of speeds and angles of attack to fully define their hydrodynamic characteristics. The models include aspect ratios of 1.0 to 5.0, sweep angles of 0 to 56.3°, taper ratios of 0 to 1.00, design lift coefficients of 0 to .350, and were tested at cavitation numbers of .029 to .145.

Lift, drag, pitching moment, and strut base pressure were measured for all models, and cavity pressure and foil base pressure were measured for the supercavitating models. The foil cavity pressure was measured by means of a static pressure tap centrally located on the upper surface of one semi-span.

Analysis of the test results was limited to the fully ventilated lift and drag data; the transition from fully wetted to fully ventilated did not cover a significant angle of attack range on any foil tested. Transition from wetted to cavitated flow on these foils was characteristically accompanied by a very high frequency vibration audible as a loud screech. A study of this "singing" phenomenon did not conclusively identify the source but gave some indication that it was associated with a stall flutter type instability.

The work of this contract has been submitted in three volumes. Volume I presents the measured results in tabular form, the correlation of results, the structural analysis, and an analysis of the "singing" phenomenon encountered during the tests. Volume II presents the measured results in graphical form.

This volume summarizes the test results as a theory for the prediction of the lift and drag for a fully cavitated hydrofoil of arbitrary section and planform with a numerical example. Measured and predicted lift and drag are compared over ranges of submergence and hydrofoil geometric parameters as a measure of the reliability of the prediction procedure.

CONCLUSIONS

Classic ventilated hydrofoil theory provides adequate correlation for these results if a modified value for the cross-flow lift coefficient is accepted. With the modified cross-flow lift coefficient, the correlation of the fifty-nine measured lift and drag curves with classic ventilated hydrofoil theory may be summarized statistically as a prediction reliability   (+ error indicates measurement higher than predicted):

	Mean Error	Probable Error
Lift Coefficient	-.002	+.012
Drag Coefficient	+.0012	+.0028

SYMBOLS

NOTE: All Dimensions in Ft./#/Sec./Radians Unless Otherwise Noted.

A	Aspect Ratio.
A_n	Section Coefficient. See Eqs. 2 and 3.
$A_o{}'$	Section Coefficient. See Eq. 1.
b	Span.
c	Chord.
$\bar{c}$	Chord in Transformed Plane = $\sqrt{c}$.
C_D	Total Foil Drag $= C_{D_L} + C_f$.
C_f	Schoenherr Drag Coefficient.
C_{D_L}	Drag Coefficient Due to Lift. See Eq. 12.
C_L	Lift Coefficient.
C_{L_1}	Lift Coefficient Due to Camber, Angle of Attack, and Cavitation Number. See Eq. 9.
C_{L_c}	Lift Coefficient Due to Crossflow. See Eq. 9.
C_ℓ	Section Lift Coefficient.
C_{ℓ_α}	Section Lift Curve Slope. See Fig. 2.
C_{ℓ_i}	Design Section Lift Coefficient.
ΔC_ℓ	Lift Coefficient Due to Cavitation Number. See Fig. 3.
d	Submergence.
E	Jones Edge Correction Factor. See Eq. 10.
K_b	Biplane Factor For Surface Effect. See Fig. 5.
t	Section Thickness.
x	Distance From Leading Edge.
$\bar{x}$	x in Transformed Plane $= \sqrt{x}$
y	Section Lower Surface Ordinate.
$\bar{y}$	y in Transformed Plane.
α	Foil Angle of Attack.
α_c	Camber Equivalent Angle of Attack, See Eq. 6 and Fig. 1.
α_i	Induced Angle of Attack. See Eq. 11.
α_o	$\tan^{-1}\left(\dfrac{-y\ell}{c}\right)_{T.E.} - A_o{}'$
α_s	Section Angle of Attack $= \alpha + A_o{}' + \alpha_c - \alpha_i$.
γ	Half-Angle Subtended by Circular Arc Section.
θ	Parameter Defining Distance Along Chord. See Eq. 5.

Δ Foil Sweep. For c/4 Line Unless Otherwise Specified.

λ Taper Ratio.

σ Cavitation Number.

σ_c Cavitation Number Based on Cavity Pressure.

τ Planform Correction Factor. See Fig. 6.

SUBSCRIPTS

ℓ Lower.

T.E.   Trailing Edge.

∞ At Infinite Submergence.

DISCUSSION

A. Model Description

The twenty models of this program are described in Table III and the sections employed are shown on Figure 28. Each foil, except number 7, is mounted on a single 15% thick, blunt base parabolic strut. Foil number 7 is mounted on a twin strut combination. All the foil models have a curvature of 51 inch radius added to their ordinates to account for the streamline curvature of the Whirling Tank. This curvature is tangent to the foil chord line at 25% of the mean geometric chord of each model.

A static pressure tap is located at the base of the strut, on the base of each foil, and on the upper surface of each foil. The upper surface pressure tap is located at the 80% chord station on the middle of one semi-span.

B. <u>Lift and Drag Prediction</u>

Classic supercavitating hydrofoil theory, as presented by Johnson in Reference 1, was the basis for the correlation of these results. A number of variations of the classic theory were applied to the data but correlation was adequate only when a modified cross-flow lift coefficient was employed. The applicable equations of Reference 1 are repeated in this section.

The section coefficients are defined by Equation (11) of Reference 1:

(1) $A_0' = -\dfrac{1}{\pi} \int_0^\pi \dfrac{d\bar{y}}{d\bar{x}} \, d\theta$

(2) $A_1 = \dfrac{2}{\pi} \int_0^\pi \dfrac{d\bar{y}}{d\bar{x}} \cos\theta \, d\theta$

(3) $A_2 = \dfrac{2}{\pi} \int_0^\pi \dfrac{d\bar{y}}{d\bar{x}} \cos 2\theta \, d\theta$

where it is noted from Equation (5) of Reference 1 that

(4) $\left(\dfrac{d\bar{y}}{d\bar{x}}\right)_{\bar{x}} = \left(\dfrac{dy}{dx}\right)_x$

where $\bar{x} = \sqrt{x}$

and by definition

(5) $\theta = \cos^{-1}\left(1 - 2\dfrac{\bar{x}}{c}\right)$

Note that the section coefficients are poorly defined at the leading edge (e.g. the 1% chord station is at nearly 20% of the θ scale) and that these coefficients are not defined at all for sections of infinite slope such as parabolic sections or sections cambered on the a = 1.0 mean line. Note further, however, that parabolic thickness distributions do not contribute to section angle of attack; that is

$$A_0' + \alpha_{c_\infty} = A_0' + A_1 - \dfrac{A_2}{2} = 0$$

for parabolic thickness distribution.

Where a section presents any significant curvature near the leading edge, therefore, accuracy is improved by subtracting an arbitrary amount of parabolic thickness distribution from the section ordinates. In practice it has proven convenient to subtract that amount of parabolic thickness which provides a zero ordinate at the first specified chord station.

By definition, the angle-of-attack increase due to camber is given at infinite submergence by

$$(6) \quad \alpha_{c_\infty} = A_1 - \frac{A_2}{2}$$

The free surface effect on the section camber, $\alpha_c / \alpha_{c_\infty}$,

may be taken from Figure 11 of Reference 1 which is presented here as Figure 1 for convenience. The curve for the Tulin-Burkart section was employed in the correlations of this report.

The section lift curve slope, C_{ℓ_α}, is taken from Figure 2

of Reference 1 which is presented here as Figure 2 for convenience.

The increment in lift coefficient added for finite cavitation number is that of Equation (4), of Reference 2 for a flat plate which is graphically presented in Figures 3 and 6 of Reference 2 and in Figure 3 of this report. The Auslaender equation (Equation 18 of Reference 3)

$$(7) \quad \Delta C_\ell = \sigma C_{\ell_{\sigma=0}} + \frac{\sigma^2 (1 - \frac{\sigma}{2})}{4 C_{\ell_{\sigma=0}}} \qquad (d = \infty, \ \sigma < .4)$$

$$\text{where} \quad \Delta C_\ell = C_{\ell_\sigma} - C_{\ell_{\sigma=0}}$$

is compared with the Wu equation at two angles of attack for infinite aspect ratio on Figure 4. The difference between the two equations is a function of submergence, angle of attack, and planform and it is difficult to generalize. The two equations differ significantly only at cavitation numbers greater than .10 and section angles of attack less than about 6°. This operating condition was poorly covered by the configurations tested but gave some indication that the Auslaender equation is preferable for this region.

The section lift is given by

$$(8) \quad C_\ell = C_{\ell_\alpha} (\alpha + A_0' + \alpha_c) + \Delta C_\ell$$

and the three-dimensional lift coefficient is given by

$$(9) \quad C_L = C_{L_1} + C_{L_c}$$

where:

$$C_{L_1} = \frac{C_{\ell_\alpha} \cos \Lambda c/2}{E} \, \alpha_s + \Delta C_\ell$$

$$C_{L_c} = \frac{2.4}{AE} (1+\sigma) \sin^2 \alpha_{cr} \cos \alpha'_{cr}$$

$$\alpha_s = \alpha + A'_o + \alpha_c - \alpha_i$$

$$\alpha_{cr} = \alpha + A'_o + \alpha_c + \alpha_o$$

$$\alpha'_{cr} = \alpha + A'_o + \alpha_o$$

The constant, 2.4, in the cross-flow lift coefficient expression was established on Figure 5 by favoring the results obtained at the higher values of the cross-flow lift parameter, $(1 + \sigma) \sin^2\alpha_{cr}\cos\alpha'_{cr}/AE$. All the data obtained for cross-flow lift parameters greater than .02 are presented on Figure 5 though only representative results are presented for lower values of the parameter. Additional testing on an extended range of the cross-flow lift parameter would be desirable for further substantiation of this important constant.

The Jones edge correction factor, E, may be taken from Figure 6 for foils having unswept half-chord lines or, in the general case, is given by

$$(10) \quad E = \frac{2\lambda}{A(1+\lambda)} + \frac{1}{2}\sqrt{1 + \left[\tan \Lambda + \frac{1-\lambda}{A(1+\lambda)}\right]^2} + \frac{1}{2}\sqrt{1 + \left[\tan \Lambda - \frac{3(1-\lambda)}{A(1+\lambda)}\right]^2}$$

The induced angle of attack is given by

$$(11) \quad \alpha_i = \frac{C_{L_1} K_b}{\pi A} (1 + \tau)$$

where the biplane factor, K_b, and the Glauert planform correction factor, τ, may be taken from Figures 7 and 8.

The drag due to lift is given by

$$(12) \quad C_{D_L} = C_{L_1} \tan(\alpha + A'_o) + C_{L_c} \tan(\alpha + A'_o + \alpha_o)$$

The Schoenherr line is included in this Volume as Figure 9. Note that only the lower surface is wetted on the supercavitating hydrofoil. A roughness allowance of .0004 is suggested for prototype foils.

C. Example

Geometry (Foil No. 4, Figures 10 and 11)

Aspect Ratio, $A = 3.0$
Quarter-chord Sweep Angle, $\Lambda = 0$
Taper Ratio, $\lambda = .5$
Thickness Ratio, $t/c = .131$
Section: Parent (These specifications, from Reference 4, are not used in the performance calculations and the symbols are not employed elsewhere in the report)
Design Lift Coefficient, $C_{l_i} = .170$
Camber Index, $c_2 = .0875$
Design Angle of Attack, $\delta = 2.5^{\circ}$
Semi-parabolic thickness, $\tau = 0$
Induced Curvature Correction, $f = .0099$
Submergence, $d/c = 1.0$
Cavitation Number, $\sigma = .066$

Section Coefficients

The section is shown on Figure 10.

The chordwise distributions for $\frac{dy}{dx}$ and $\frac{d\bar{y}}{d\bar{x}} \cos n\theta$ are computed in Table I and plotted on Figures 12, 13 and 14. Integration on Figures 12, 13, and 14 yields

$$A_0' = 2.11^{\circ}$$

$$A_1 = 2.75^{\circ}$$

$$A_2 = -1.46^{\circ}$$

where it should be noted that these results differ from the computer evaluations employed in Volume I by .5% to 2.5%.

By definition:

$$\alpha_{c_{\infty}} = A_1 - A_2/2$$
$$= 2.75^{\circ} + 1.46^{\circ}/2$$
$$= 3.48^{\circ}$$

Foil Lift and Drag

The foil lift and drag curves are derived in Table II. The supporting derivations required are as follows (note that computer derived section coefficients are employed here):

$$\alpha^o_i = 57.3 \frac{C_{L_1} K_b}{\pi A} (1 + \tau)$$

$$= 57.3 \times \frac{1.16}{3\pi} \times 1.027 \, C_{L_1}$$

$$= 7.24 \, C_{L_1}$$

$$\alpha^o_o = \tan^{-1} \left(\frac{-y\ell}{C}\right)_{T.E.} - A'_o$$

$$= \tan^{-1} .0421 - 2.06^o$$

$$= .35^o$$

D. Correlations

The measured lift and drag data are compared with the predictions for each foil in Part III, Volume I. Figures 15 - 27 of this Volume make these comparisons between the members of foil families included among the twenty foils tested in order to illustrate the ability of the theory to predict the effect of individual foil parameters. The data for all these figures have been reduced to zero cavitation number for direct comparison. Strut drag and foil friction drag have been removed from the measured drags to reduce the results to drag due to lift.

Correlation with aspect ratio (Figures 15 and 20) and camber (Figures 16 and 21) is good except for the foils of least camber which differ significantly in slope on Figure 16 and in position on Figure 21. The slope disagreement occurs frequently throughout the data but is not systematic with the hydrofoil configuration. Note that Foil No. 7 was excluded from Figure 20 because the struts failed before drag tares could be obtained.

The results for taper ratio effect (Figures 17 and 22) verify qualitatively that taper ratio becomes more significant as it approaches unity. The range of sweeps provided for the foils incorporating the parent section was too limited to present a significant sweep effect (Figures 18 and 23).

The taper ratio effect and the sweep effect (for small sweep angles) are both of the same order as the effect of the speed on the foil characteristics and further experience with this speed effect would be required to provide a data precision which would measure the effects of taper ratio and moderate sweep. The source for the

speed effect cannot be positively identified from the data. It is not a Froude Number effect because Froude Number is independent of speed in the Whirling tank. Observation of the flow about the Langley Model No. 5 in the water tunnel of Hydronautics, Inc. reveals persistent wetted flow in regions influenced by the strut and by the tip vortex and the data is consistent with lingering wetted flow followed by a more typical Reynolds Number effect.

The effect of submergence was negligible for all foils tested (Figures 19 and 24), the section lift curve slope effect being almost exactly offset by the camber effect.

Drag data throughout this report have been presented as polar drag curves because it is the foil lift/drag ratio which is of primary interest. For information, however, typical curves of drag vs. angle of attack are presented on Figures 25, 26, and 27. Figures 25 and 26 do not add anything to the interpretation of Figures 20 and 21, being virtual cross-plots of those figures. Figure 27 is presented as evidence that the poor correlation for Foil Nos. 16 and 17 of Figure 26 is not systematic with design lift coefficient.

REFERENCES

1. NACA RM L57I16, 1957, "Theoretical And Experimental Investigation of Arbitrary Aspect Ratio, Supercavitating Hydrofoils Operating Near The Free Water Surface", Virgil E. Johnson, Jr.

2. California Institute of Technology Report No. 47-4, 1955, "Comparison Of The Characteristics Of A Hydrofoil Under Cavitating And Non-cavitating Operation", T. Yao-Tsu Wu and Bryne Perry.

3. Hydronautics, Inc., Technical Report 001-7, 1962, "Low Drag Supercavitating Sections", Jakob Auslaender.

4. Hydronautics, Inc., Letter to Preliminary Design Branch, BuShips, 10 November 1960, "Section Ordinates of a Supercavitating Single Strut Wing Proposed for Experimental Investigation", Virgil E. Johnson, Jr.

TABLES

1	2	3	4	5	6	7
$\frac{x}{c}$	$-\frac{y_1}{c}$	$\Delta\frac{x}{c}$	$-\Delta\frac{y}{c}$	$-\left(\frac{d\bar{y}}{d\bar{x}}\right)_{\bar{x}}$	$\frac{\bar{x}}{c}$	$2\frac{\bar{x}}{c}$
0	0			(.008)	0	0
.025	.0003	.050	.0004	.008	.1580	.3160
.05	.0004	.050	.0004	.008	.2237	.4474
.075	.0007	.050	.0004	.008	.2735	.5470
.1	.0008	.075	.0006	.008	.3162	.6324
.15	.0013	.100	.0009	.009	.7873	.7746
.2	.0017		.0010	.010	.4472	.8944
.25	.0023		.0011	.011	.5000	1.000
.3	.0028		.0013	.013	.5477	1.0954
.35	.0036		.0017	.017	.5920	1.184
.4	.0045		.0021	.021	.632	1.1264
.45	.0057		.0027	.027	.671	1.342
.5	.0072		.0033	.033	.707	1.414
.55	.0090		.0038	.038	.742	1.484
.6	.0110		.0048	.048	.775	1.550
.65	.0134		.0051	.051	.806	1.612
.7	.0161		.0058	.058	.837	1.674
.75	.0192		.0067	.067	.866	1.732
.8	.0228		.0077	.077	.894	1.788
.85	.0269		.0086	.086	.922	1.844
.9	.0314		.0096	.096	.949	1.898
.95	.0365		.0107	.107	.975	1.950
1.00	.0421	.100		(.1245)	1.000	2.000

NOTE: Section is shown on Figure 10.

1, 2   Lower Surface Section Ordinates.

3, 4   Co-ordinate Differences

5   (4)/(3) Extrapolation for x/c = 0 & 1. See Figure 11.

6     $\sqrt{(1)}$

7   2 x (6)

TABLE I

OEFFICIENT PARAMETERS

ON $\quad C_{l_i} = .170 \quad t/c = .131$

	8	9	10	11	12	13	14
	$\cos \theta$	θ°	θ	$d\bar{y}/d\bar{x}$ x $\cos \theta$	$2\theta^{\circ}$	$\cos 2\theta$	$d\bar{y}/d\bar{x}$ x $\cos 2\theta$
	1.000	0	0	-.00800	0	1	-.00800
	.6740	46.9	.818	-.00538	93.8	- .0663	.00053
	.5526	56.5	.986	-.00442	113.0	- .3905	.003125
	.4530	63.1	1.102	-.00362	126.2	- .591	.004725
	.3676	68.45	1.193	-.002935	136.9	- .730	.00584
	.2254	77.0	1.343	-.00203	154.0	- .899	.00808
	.1056	83.95	1.463	-.001056	167.9	- .979	.00979
	0	90.0	1.57	0	180.0	-1.000	.01100
	- .0954	95.5	1.666	.00124	191.0	- .981	.01275
	- .184	100.6	1.753	.00313	201.2	- .933	.01595
	- .264	105.3	1.837	.00554	210.6	- .860	.01805
	- .342	110.0	1.920	.00923	220.0	- .766	.0207
	- .414	114.4	1.997	.01365	228.8	- .695	.0217
	- .484	118.85	2.07	.01840	237.7	- .534	.0203
	- .550	123.4	2.155	.0242	246.8	- .394	.01735
	- .612	127.6	2.255	.0312	255.2	- .2555	.01303
	- .674	132.3	2.31	.0391	264.6	- .0941	.00546
	- .732	137.0	2.39	.0490	274.0	.0698	-.00468
	- .788	142.0	2.48	.0607	284.0	.242	-.01863
	- .844	147.5	2.575	.0725	295.0	.423	-.0363
	- .898	153.8	2.68	.0862	307.6	.610	-.0586
	- .950	161.7	2.82	.1015	323.4	.803	-.0858
	-1.000	180.0	3.14	.1245	360.0	1.000	-.1245

8	1-(7)		13	cos (12)
9	$\cos^{-1}$ (8)		14	(5) x (13)
10	(9)/57.3			
11	(5) x (8)			
12	2 x (9)			

1	2	3	4	5	6	7	8	9	
α_s °	$\dfrac{C_{l_\alpha}}{\text{DEG}}$	$C_{l_{\sigma=0}}$	$\dfrac{C_{l_{\sigma=0}}}{E}$	ΔC_l	C_{L_1}	α_i DEG	$\alpha_i - A'_o - \alpha_c$ DEG	α DEG	α_i
8	.0305	.244	.188	.020	.208	1.51	-3.51	4.49	
12	.0281	.337	.262		.282	2.04	-2.98	9.02	
16	.0260	.416	.321		.341	2.47	-2.55	13.45	
20	.0236	.472	.363	↓	.383	2.77	-2.25	17.75	

1. Arbitrary

2. **Figure 2**

3. (1) x (2)

4. .775 x (3)
   (c/2 Sweep is Neglected)

5. **Figure 3**

6. (4) + (5)

7. 7.27 x (6)

8. From Figure 1, $\dfrac{\alpha_c}{\alpha_{c_\infty}} = .84$

   $\alpha_c = .84 \times 3.53 = 2.96°$

   (8) = (7) - 2.06 - 2.96

   (Computer Evaluations Employed)

9. (1) + (8)

10. (7) + .35°

Foil Number	Aspect Ratio A	c/4 Sweep Angle-Deg. Λ	Taper Ratio λ	Thickness Ratio t/c	Design Lift Coeff. C_{l_i}	Foil Section	d
1	3.0	0	1.00	.118	0	Wedge	
2	3.0	0	1.00	.117	.275	Tulin	
3	3.0	0	.30	.131	.170	Parent	
4	3.0	0	.50	.131	.170	Parent	
5	3.0	0	1.00	.131	.170	Parent	
6	1.0	0	1.00	.131	.170	Parent	
7	5.0	0	1.00	.131	.170	Parent	
8	3.0	10.0	.30	.131	.170	Parent	
9	3.0	20.0	.30	.131	.170	Parent	
10	2.0	56.3	0	.030	0	Flat	
11	2.0	24.2	.25	.030	0	Flat	
12	3.0	45.0	0	.030	0	Flat	
13	3.0	16.7	.25	.030	0	Flat	
14	3.0	45.0	0	.060	.200	Parabolic	
15	3.0	16.7	.25	.060	.200	Parabolic	
16	3.0	0	.50	.071	.059	Parent	
17	3.0	0	.50	.103	.117	Parent	
18	3.0	0	.50	.158	.230	Parent	
19	3.0	0	.50	.180	.287	Parent	
20	3.0	0	.50	.203	.350	Parent	

TABLE III

FOIL GEOMETRY

Nominal Cavitation No. σ_c			Velocity Range Knots	Angle of Attack Range	Comments
/c = .75	d/c = 1.00	d/c = 1.25			
.048	.063	.078	40 - 80	0° to 10°	
-	.088	.110	40 - 70	1° to 12°	Model failed at 70 knots
.053	.069	.085	40 - 80	-1.5° to 3°	
.050	.066	.081	40 - 80	-2° to 7°	
.048	.064	.078	40 - 80	-1° to 9°	
.084	.110	.145	40 - 70	-1° to 11°	Mounting screw failure at 70
.029	.039	.048	40 - 70	-2° to 7°	Twin strut model - failed at
.053	.069	.085	40 - 80	-2° to 8°	80 knots.
.053	.069	.085	40 - 80	-2° to 8°	
.076	.097	.121	40 - 45	-1° to 12°	Model failed at 45 knots
.077	.101	.125	40 - 80	-1° to 12°	Model failed at 80 knots
.062	.081	.101	40 - 80	-.5° to 9°	
.053	.071	.088	40 - 80	0° to 10°	
.063	.084	.103	40 - 80	-2° to 7°	
.053	.071	.088	40 - 80	-2° to 9°	
.049	.065	.079	40 - 80	-1° to 7°	
.049	.065	.079	40 - 96	-1° to 8°	
.049	.064	.080	40 - 95	-2° to 8°	
.039	.051	.063	40 - 96	-2.5° to 8°	
.039	.051	.062	40 - 95	-2° to 9°	

FIGURES

FIGURES (Cont'd.)

FIGURE 1 EFFECTIVE ANGLE OF ATTACK DUE TO CAMBER, α_c vs. SUBMERGENCE
From Figure 11 of Ref. 1

Circular-Arc Section, $\alpha_o = \dfrac{\gamma}{8}$, $\alpha_{c_\infty} = \dfrac{9}{16}\gamma$

Five Term Section

Three Term Section

Tulin-Burkart Section

$\dfrac{\alpha_c}{\alpha_{c_\infty}}$

Ratio of Depth of Submersion to Chord, d/c
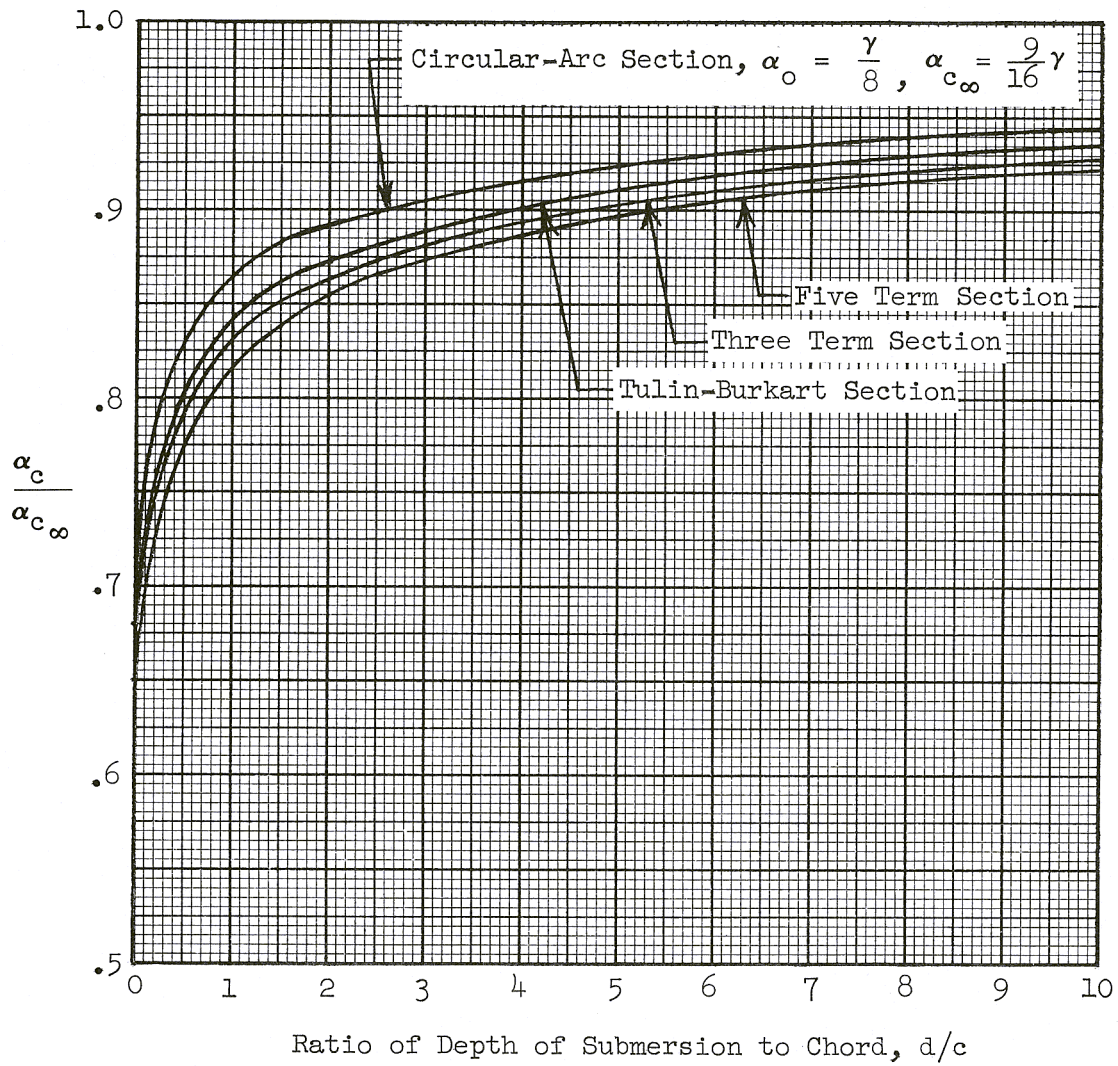
FIGURE 2 SECTION LIFT CURVE SLOPE VS. SUBMERGENCE

From Figure 2 of Ref. 1

Figure showing Section Lift Curve Slope, C_{l_α} – /Radian vs. Ratio of Depth of Submersion to Chord, d/c, with curves labeled α_s^o = 0, 4, 8, 12, 16, 20, 24, 28, 32, 36, 45, 60, 75, 90.
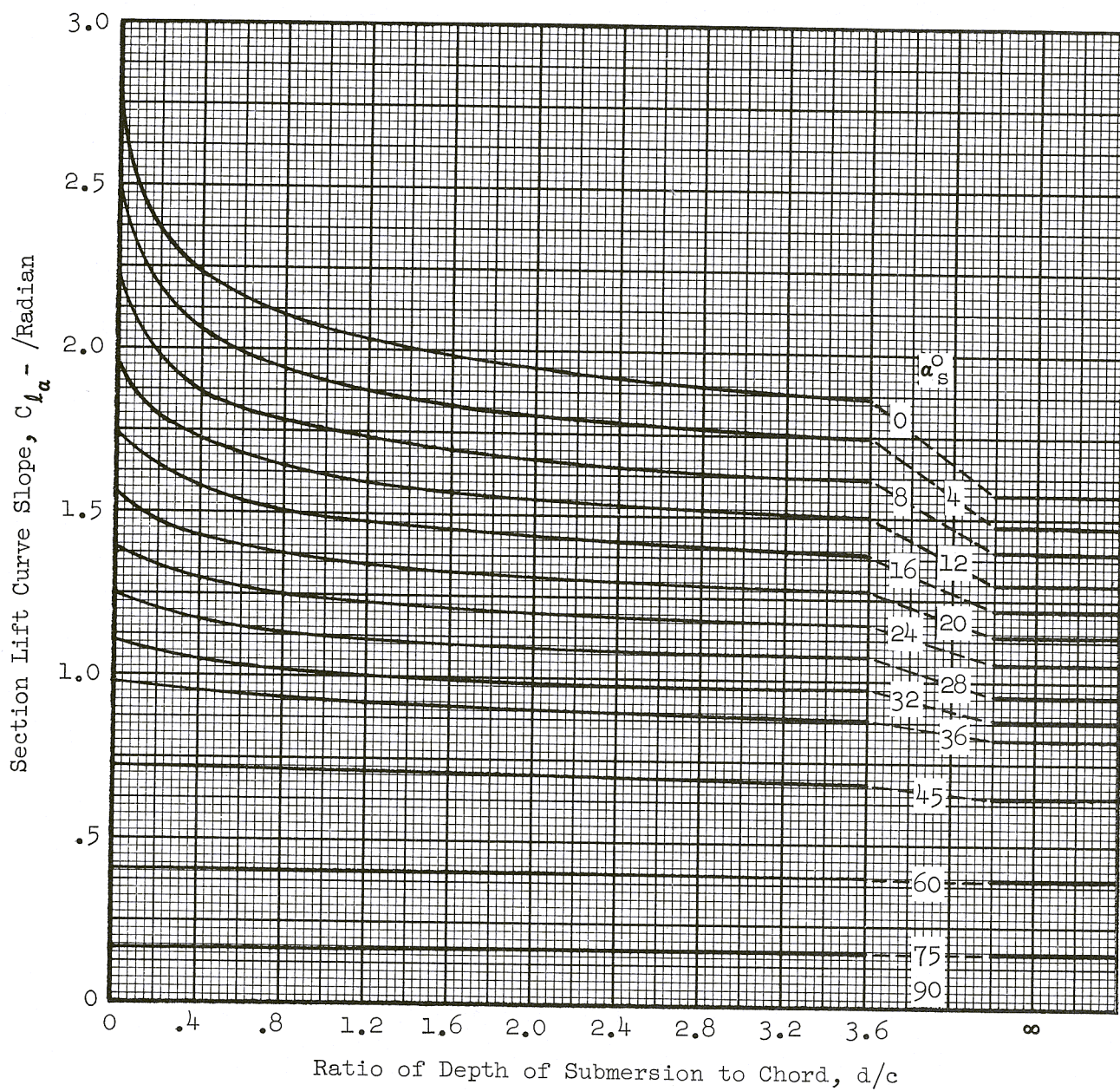
FIGURE 3 CAVITATION NUMBER LIFT INCREMENT

Flat Plate Infinite Submergence

Wu

Derived From Ref. 2
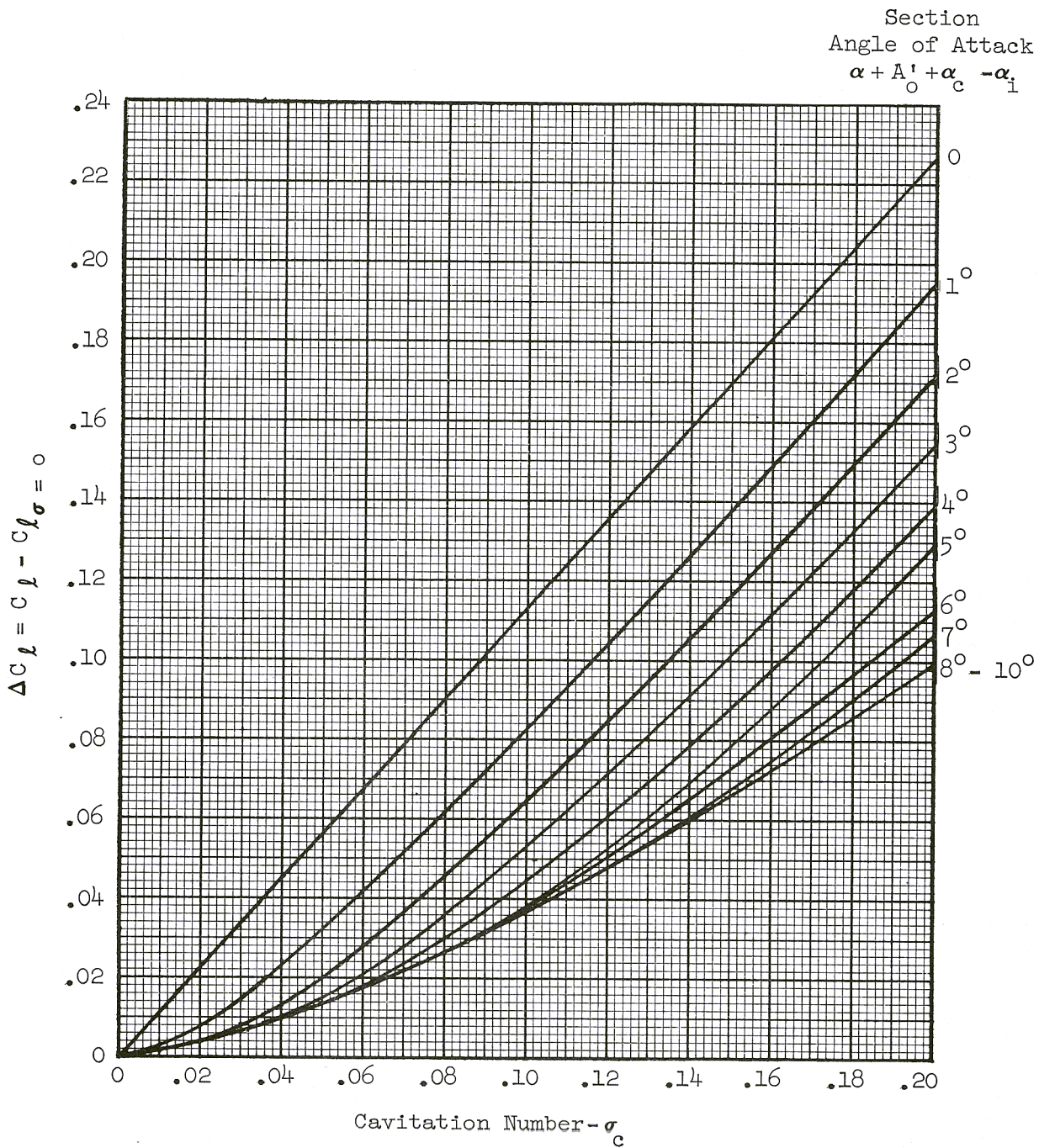
FIGURE 4   CAVITATION NUMBER LIFT INCREMENT-WU AND AUSLAENDER

Flat Plate- Infinite Aspect Ratio

$$\Delta c_\ell = c_{\ell_\sigma} - c_{\ell_{\sigma = 0}}$$

Cavitation Number- σ
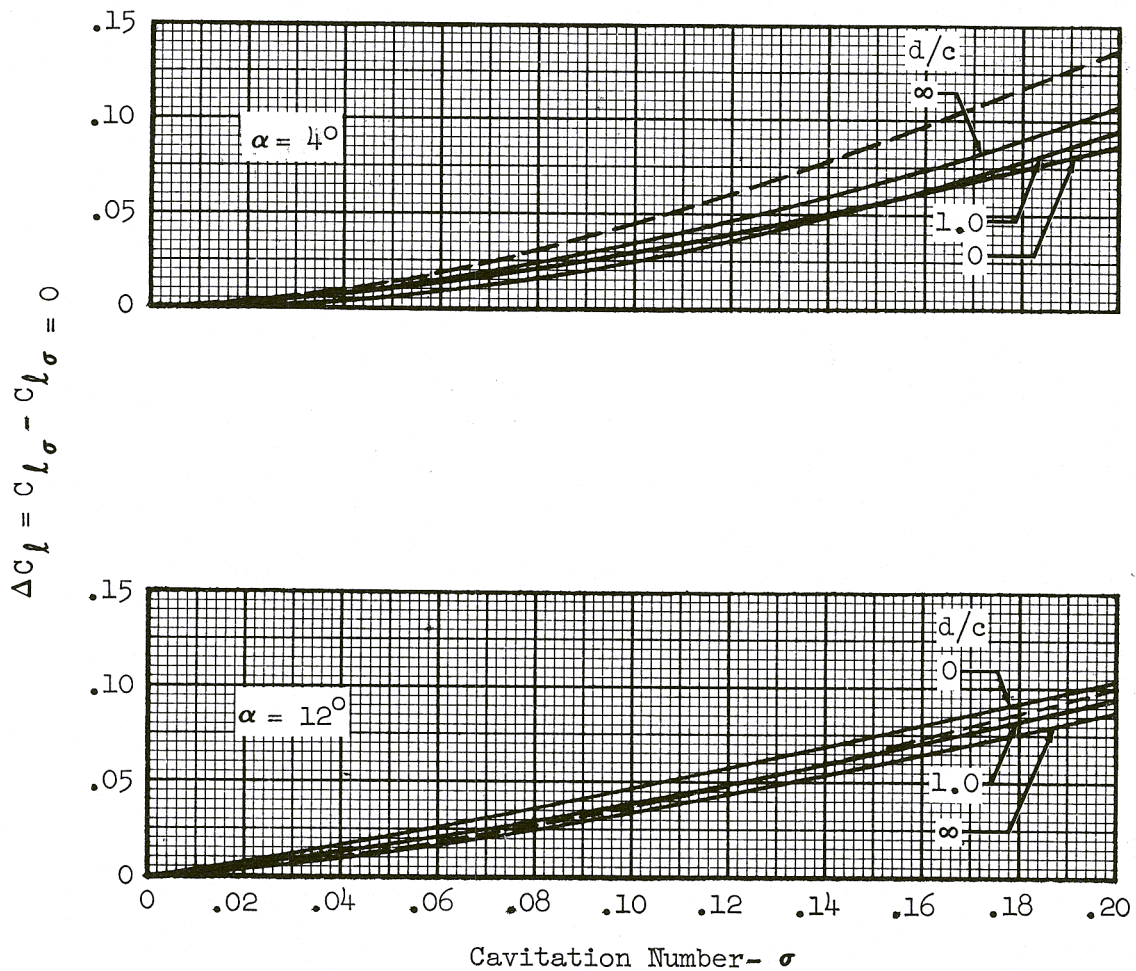
FIG. 5 CROSS-FLOW LIFT

$$\Lambda = 0$$

$$\underline{d/c = .75\text{-}1.25}$$

	Foil	Section	C_{ℓ_i}	A	λ	σ
○	1	Wedge	0	3	1.00	.048-.078
▽	2	Tulin	.275	3	1.00	.088-.110
▽	5	Parent	.170	3	1.00	.048-.078
◊	6	Parent	.170	1	1.00	.084-.145
⌂	7	Parent	.170	5	1.00	.029-.048
△	18	Parent	.230	3	.50	.049-.080
□	20	Parent	.350	3	.50	.039-.062

$$C_{L_C} = \frac{2.4}{AE}(1+\sigma)\sin^2 a_{cr}\cos a'_{cr}$$

Cross-Flow Lift, C_{L_C} — Measured C_L − Predicted C_{L_1}
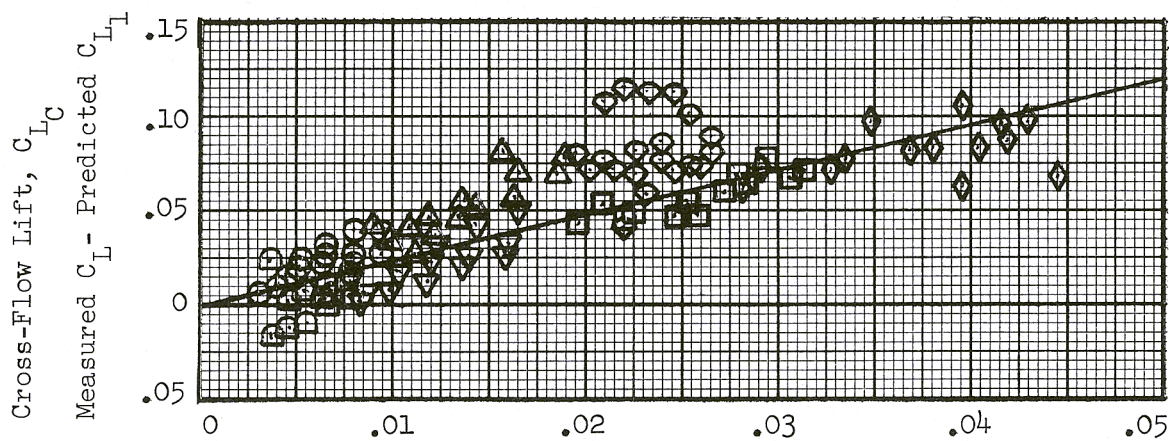
$$\frac{1+\sigma}{AE}\sin^2 a_{cr}\cos a'_{cr}$$

FIGURE 6 JONES EDGE CORRECTION FACTOR vs. ASPECT RATIO

$$E = \frac{\text{Semi-Perimeter}}{\text{Span}}$$

Unswept Half-Chord Line
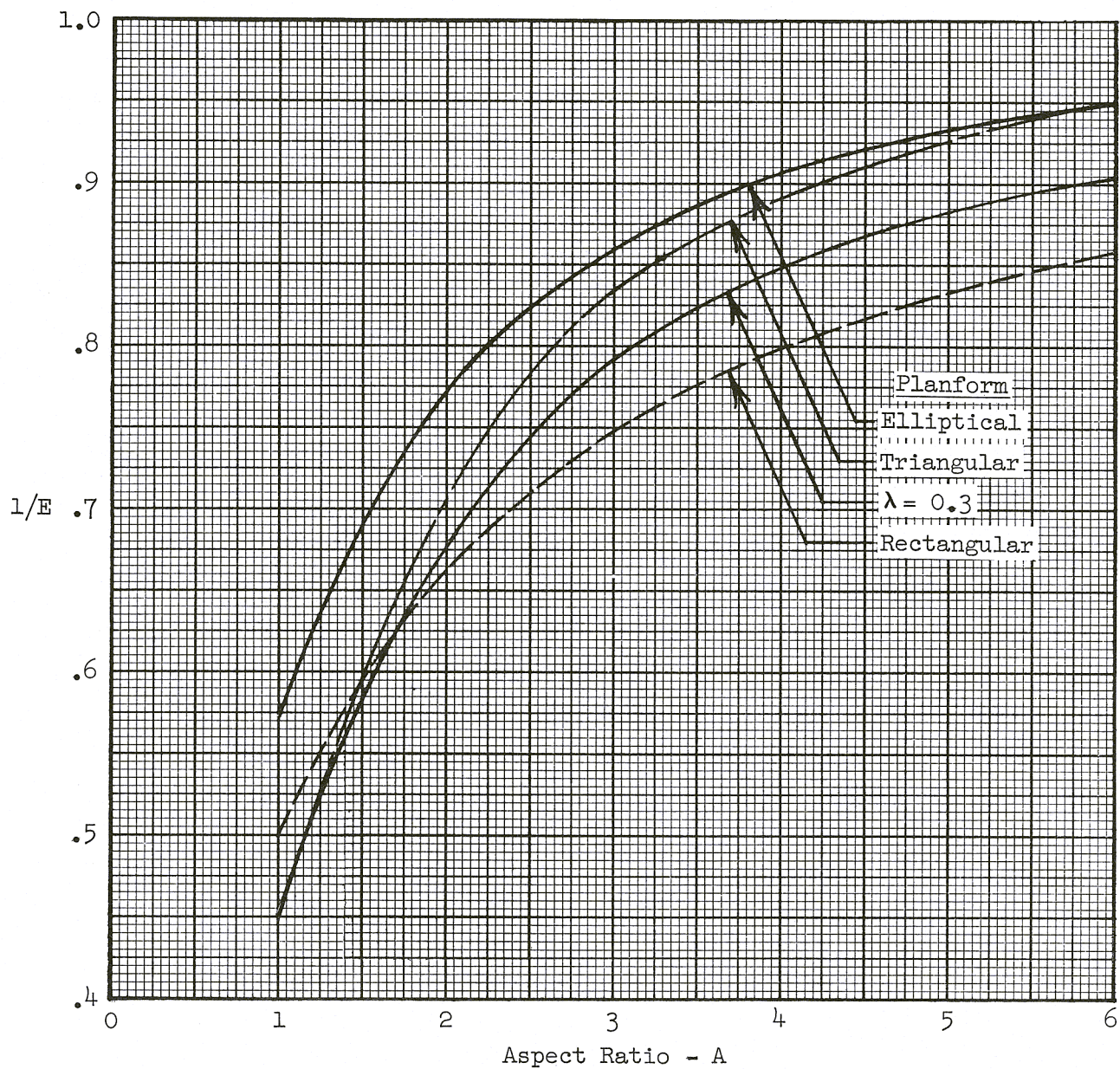
FIGURE 7   BIPLANE FACTOR, K_b
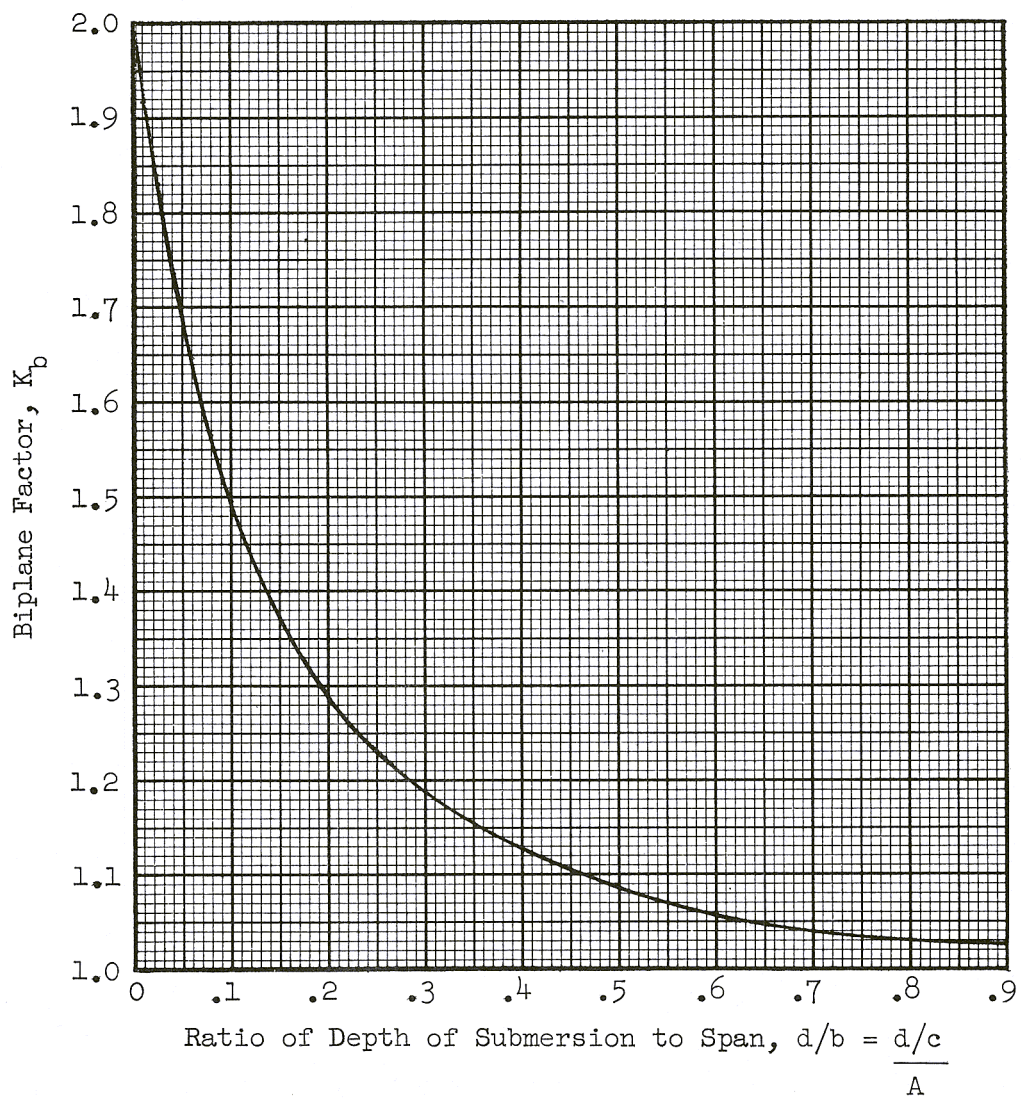
FIGURE 8   PLANFORM CORRECTION FACTOR, τ
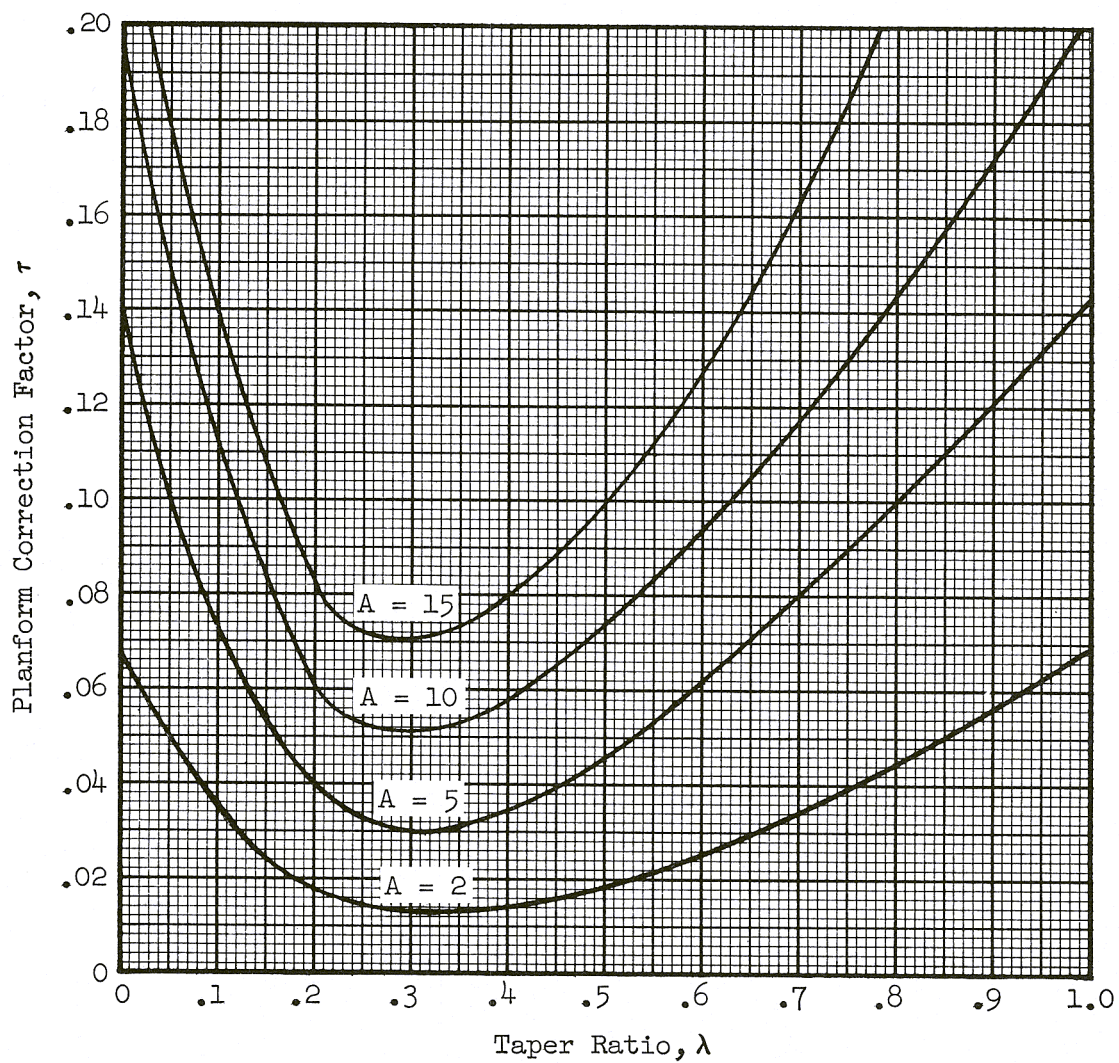
FIGURE 9 FRICTION DRAG COEFFICIENT vs. REYNOLDS NUMBER
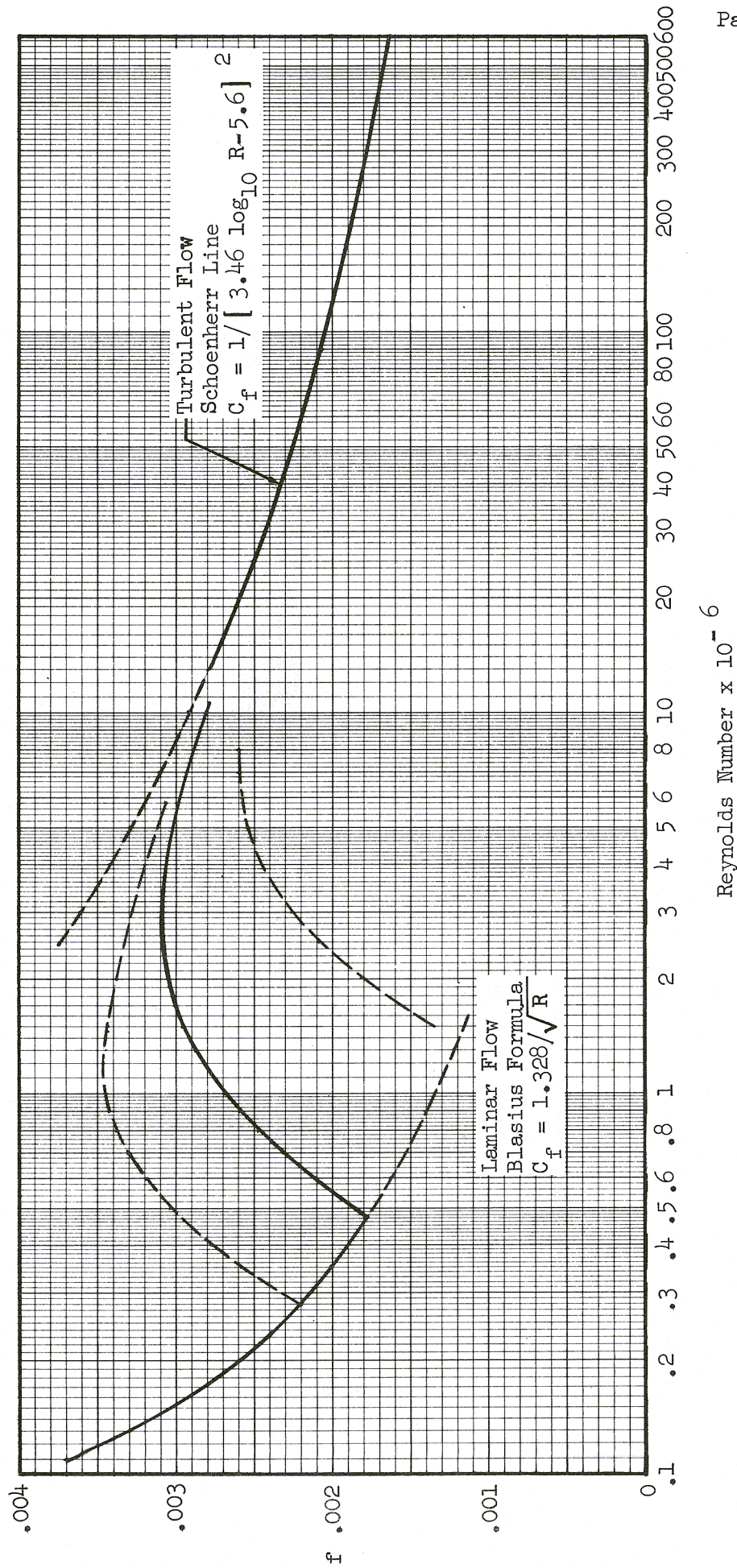
C_f Based on Wetted Area

Turbulent Flow
Schoenherr Line
$C_f = 1/[3.46 \log_{10} R - 5.6]^2$

Laminar Flow
Blasius Formula
$C_f = 1.328/\sqrt{R}$

Reynolds Number $\times 10^{-6}$

FIGURE 10 PARENT FOIL SECTION

Tulin-Burkart "Two Term" Section

Modified For One Chord Depth

$C\ell_i = .170$ $t/c = .131$
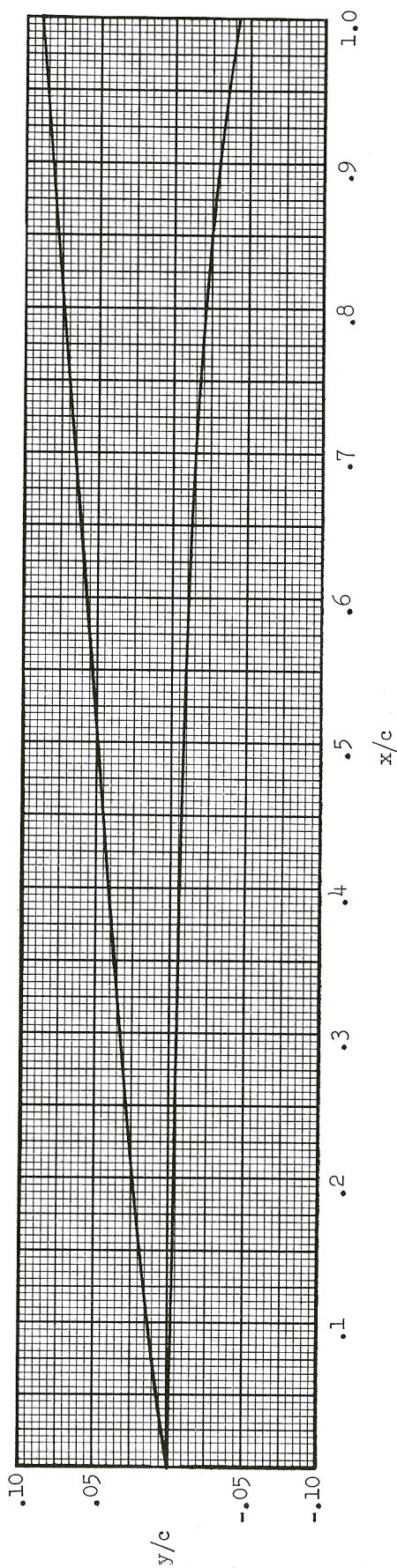
FIGURE 11   LOWER SURFACE SLOPE

Parent Foil Section
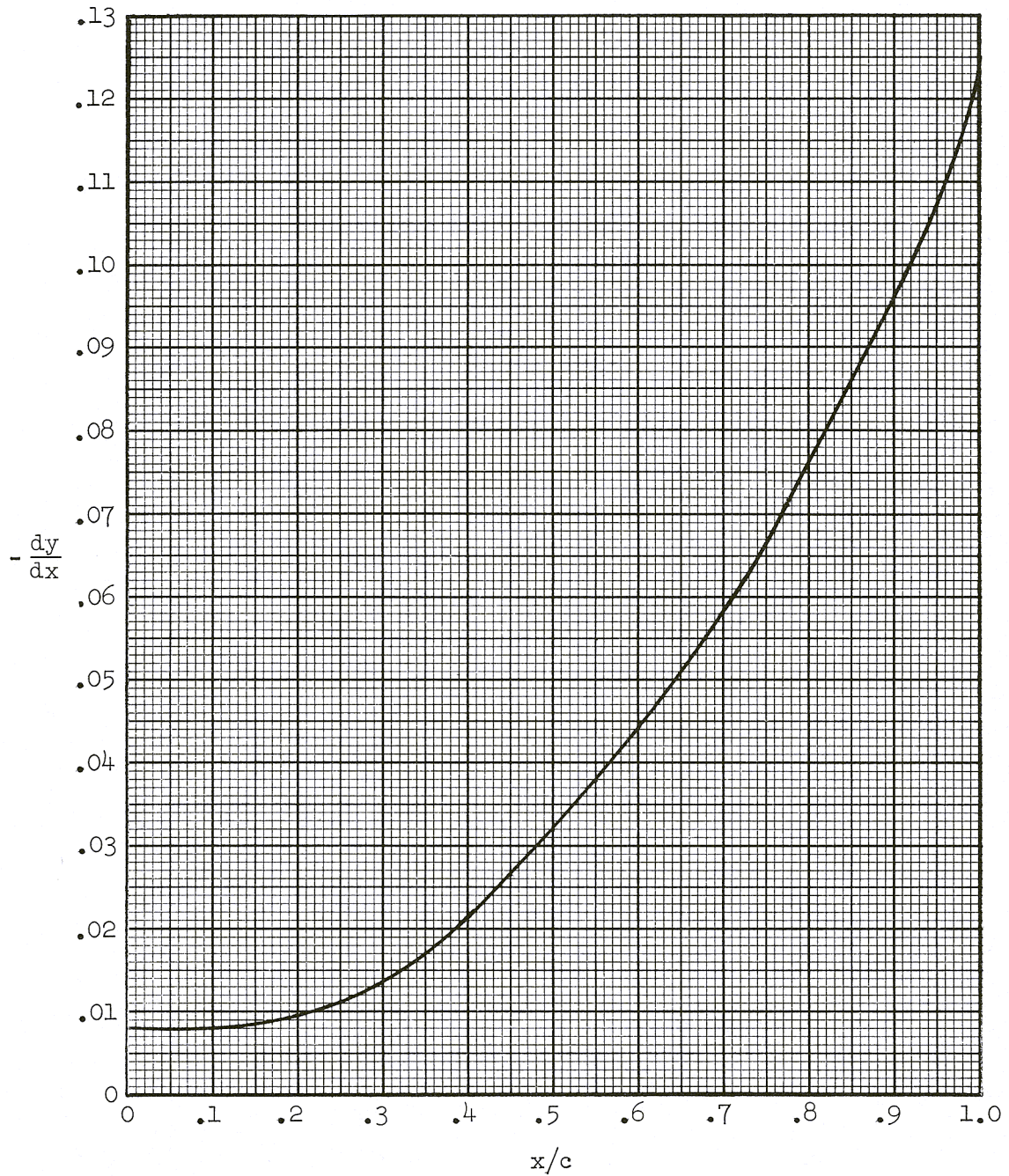
$C_{l_i} = .170$ $t/c = .131$

FIGURE 12 $d\bar{y}/d\bar{x}$ vs. θ
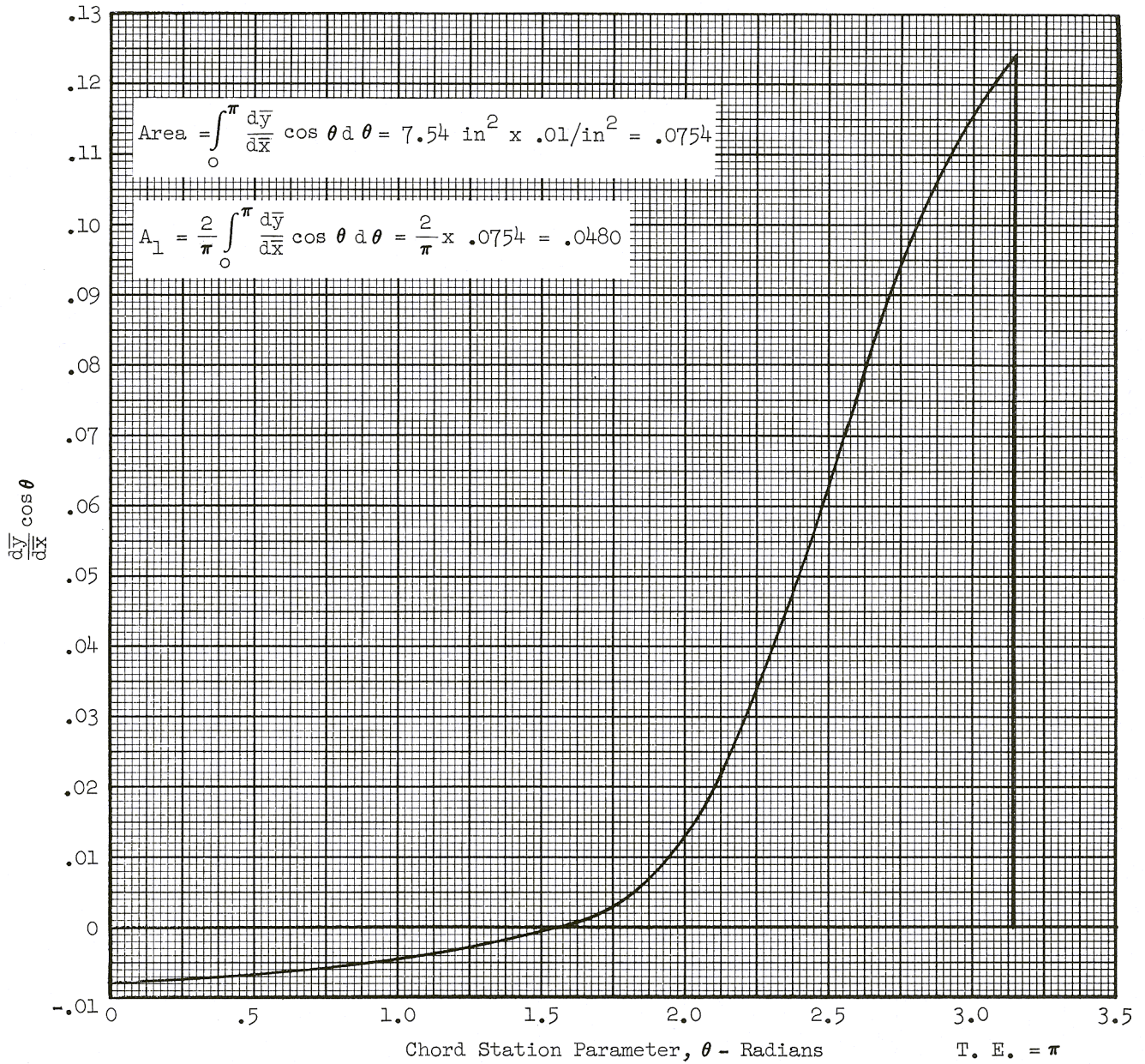
Parent Section

$C_{\ell_i} = .170 \quad t/c = .131$

$Area = \int_{0}^{\pi} \frac{d\bar{y}}{d\bar{x}} \, d\theta = -11.60 \text{ in}^2 \times .01/\text{in}^2 = -.1160$

$A'_{0} = -\frac{1}{\pi} \int_{0}^{\pi} \frac{d\bar{y}}{d\bar{x}} \, d\theta = \frac{.1160}{\pi} = .0369 = 2.11^{\circ}$

$-\frac{d\bar{y}}{d\bar{x}}$

Chord Station Parameter, θ — Radians

T. E. $= \pi$

FIGURE 13 $d\overline{y}/d\overline{x} \cos \theta$ vs. θ

Parent Section

$C_{\ell_i} = .170 \quad t/c = .131$

$\text{Area} = \int_0^{\pi} \frac{d\overline{y}}{d\overline{x}} \cos \theta \, d\theta = 7.54 \text{ in}^2 \times .01/\text{in}^2 = .0754$

$A_1 = \frac{2}{\pi} \int_0^{\pi} \frac{d\overline{y}}{d\overline{x}} \cos \theta \, d\theta = \frac{2}{\pi} \times .0754 = .0480$

Chord Station Parameter, θ – Radians   T. E. $= \pi$

$\frac{d\overline{y}}{d\overline{x}} \cos \theta$

FIGURE 14 $d\bar{y}/d\bar{x}$ COS 2θ vs. θ

Parent Section

$C_{l_i} = .170$ $t/c = .131$

T. E. $= \pi$

Area $= \int_0^\pi \dfrac{d\bar{y}}{d\bar{x}} \cos 2\theta \, d\theta = -4.0 \text{ in}^2 \times .01/\text{in}^2 = -.040$

$A_2 = \dfrac{2}{\pi} \int_0^\pi \dfrac{d\bar{y}}{d\bar{x}} \cos 2\theta \, d\theta = -.04 \times \dfrac{2}{\pi} = -.02545$

$\dfrac{d\bar{y}}{d\bar{x}} \cos 2\theta$ (vertical axis label)

Chord Station Parameter, θ - Radians
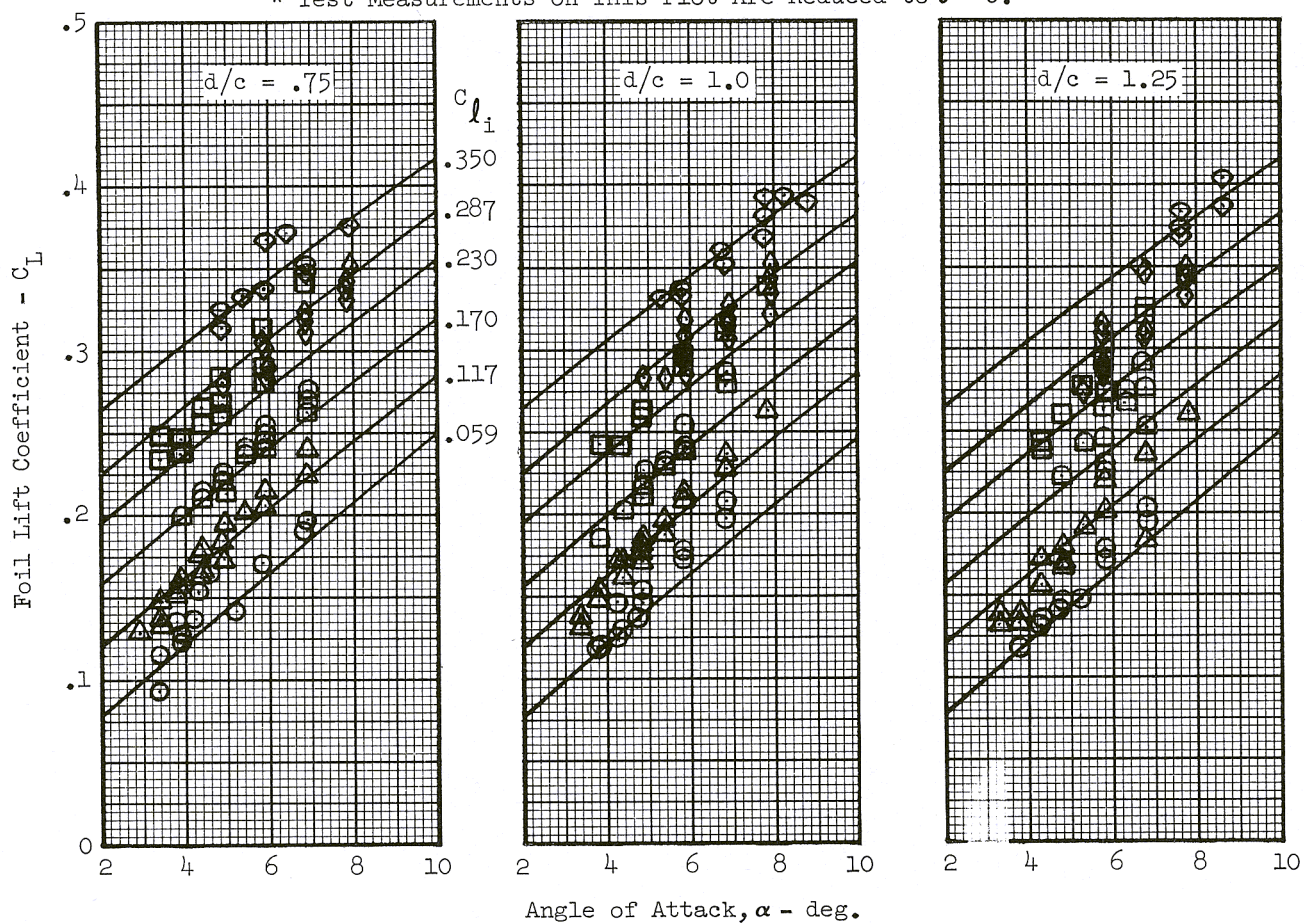
FIGURE 15 LIFT CORRELATION-ASPECT RATIO EFFECT

Parent Section ~ C_{l_i} = .170- t/c = .131

Λ = 0 λ = 1.0

σ = 0
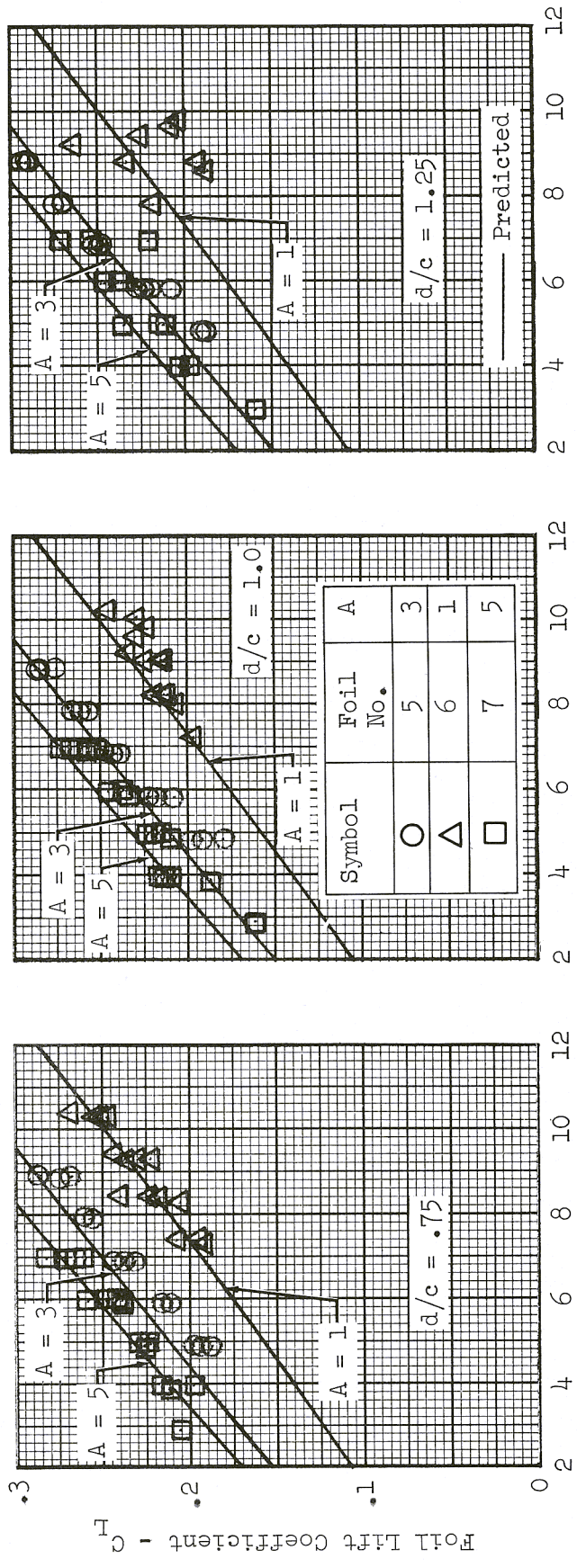
FIGURE 16 LIFT CORRELATION-CAMBER EFFECT

Parent Section

A = 3   Λ = 0   λ = .5

σ = 0

——————— Predicted

Symbol	Foil No.	c_{l_i}	t/c	Nominal σ *		
				d/c = .75	d/c = 1	d/c = 1.25
⌂	4	.170	.131	.050	.066	.081
○	16	.059	.071	.049	.065	.079
△	17	.117	.103	.049	.065	.079
□	18	.230	.158	.049	.064	.080
◇	19	.287	.180	.039	.051	.063
⬠	20	.350	.203	.039	.051	.062

* Test Measurements on This Plot Are Reduced to σ = 0.

FIGURE 17   LIFT CORRELATION-TAPER RATIO EFFECT

Parent Section - C_{l_i} = .170 - t/c = .131

Λ = 0   A = 3.0

σ = 0
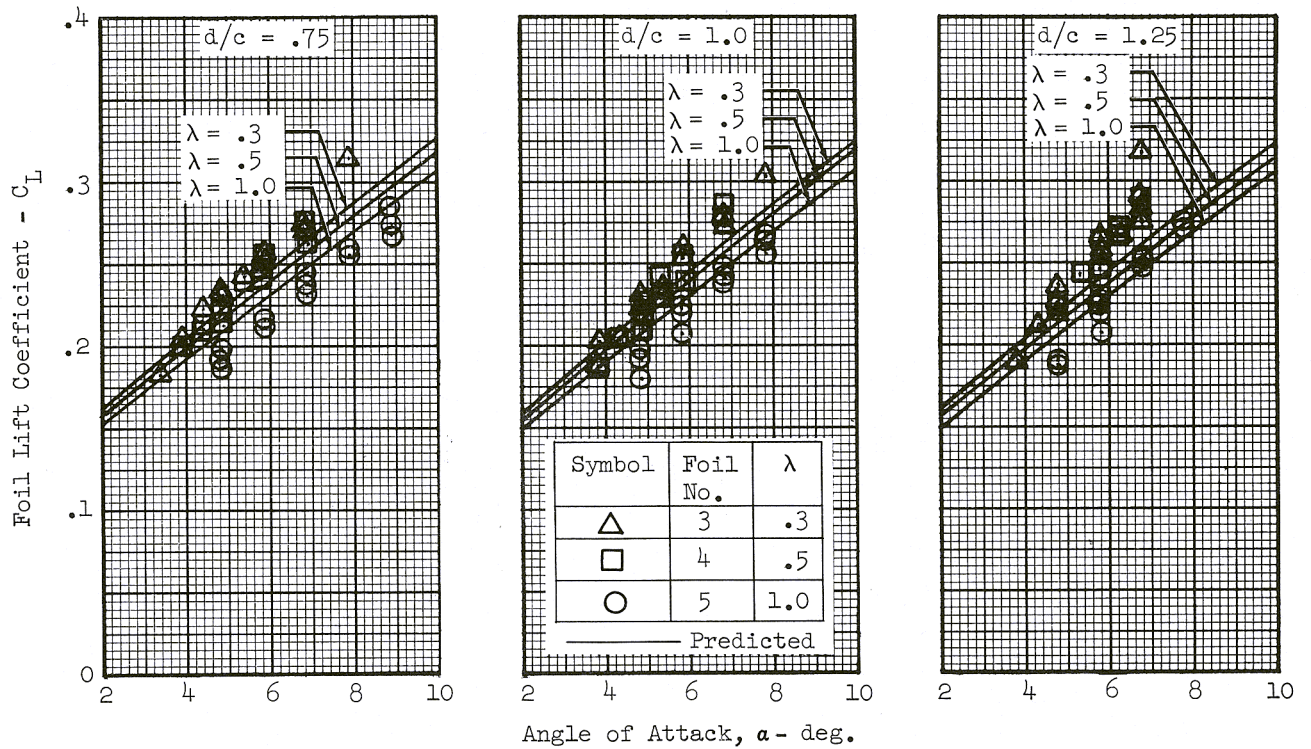
FIGURE 18 LIFT CORRELATION-SWEEP EFFECT
Parent Section - $C_{l_i} = .170 - t/c = .131$

$A = 3$ $\lambda = .3$

Prediction	Meas.	Foil No.	Λ
———	○	3	0
— — —	△	8	$10°$
— · —	□	9	$20°$
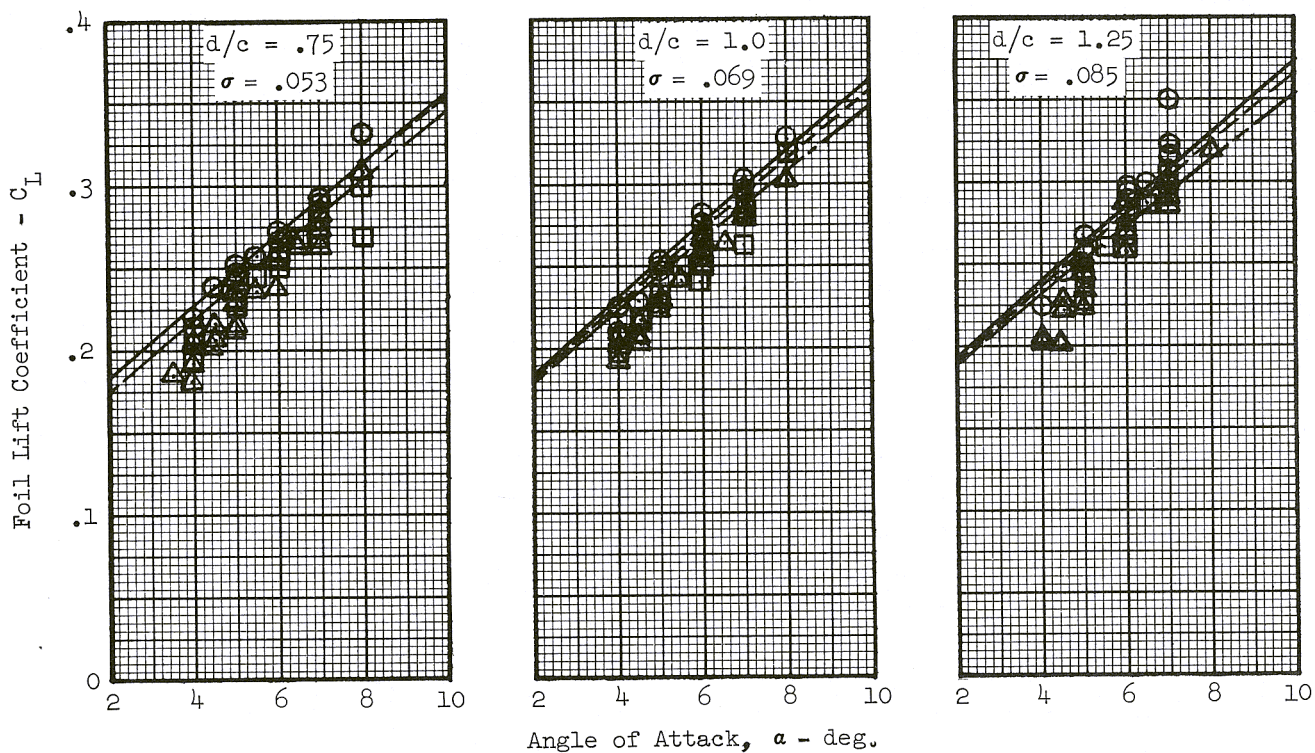
FIGURE 19   LIFT CORRELATION-SUBMERGENCE EFFECT

Parent Section

A = 3 Λ = 0 λ = .5

σ = 0

Foil No. 16 C_{ℓ_i} = .059

Foil No. 4 C_{ℓ_i} = .170

Foil No. 20 C_{ℓ_i} = .350

Typ. d/c
.75
1.0
1.25

○   d/c = .75
△   d/c = 1.0
◊   d/c = 1.25
———   Predicted

Foil Lift Coefficient – C_L

Angle of Attack, a – deg.
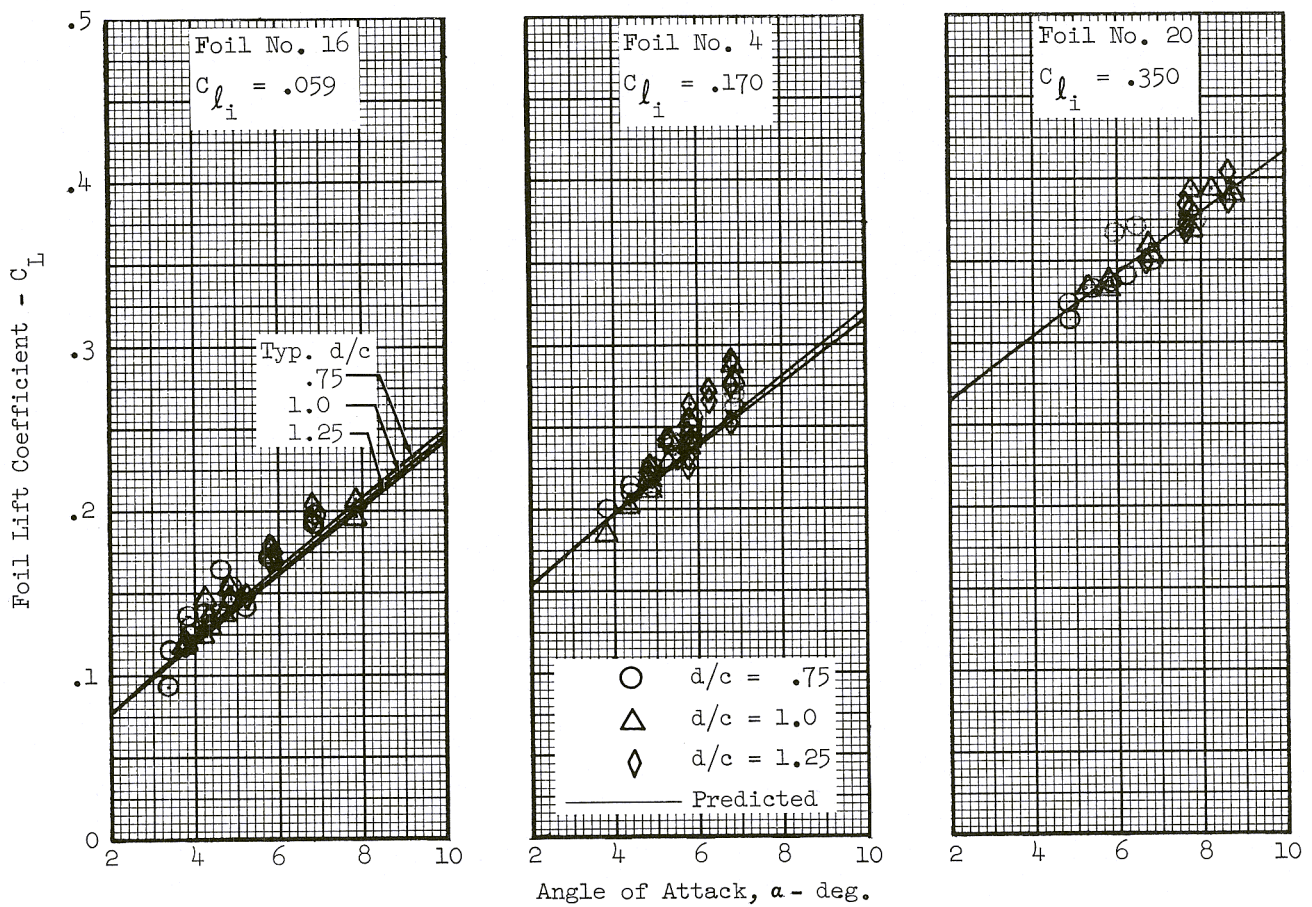
FIGURE 20 DRAG CORRELATION-ASPECT RATIO EFFECT

Parent Section - C_{ℓ_i} = .170 - t/c = .131

Λ = 0 λ = 1.0

σ = 0
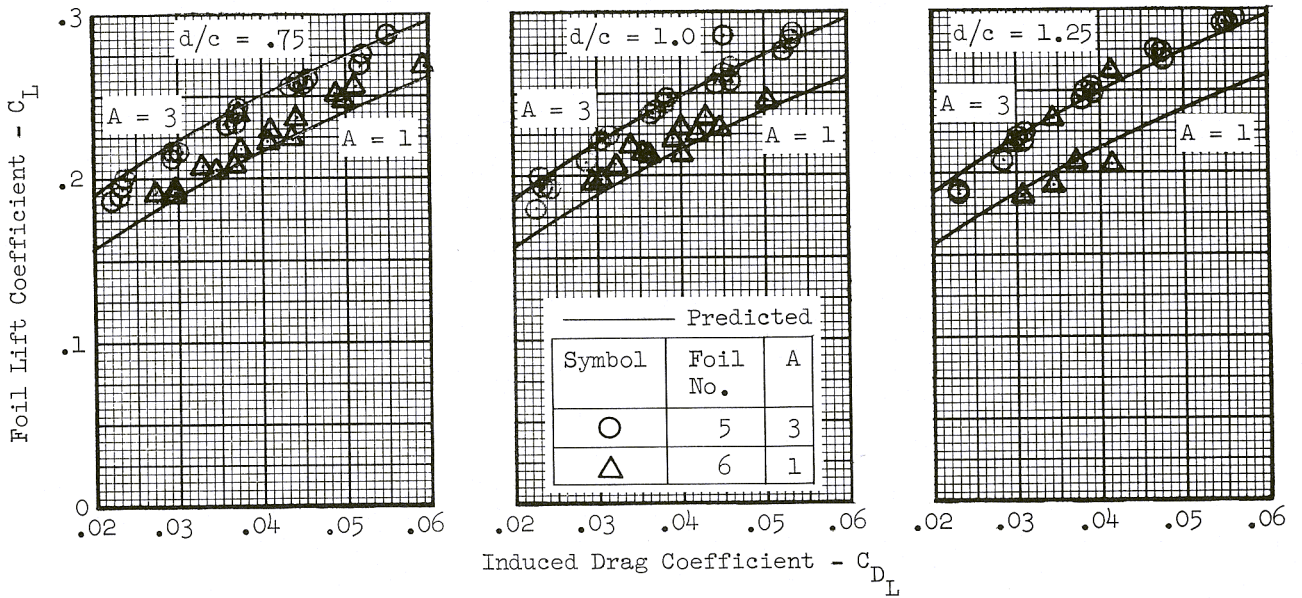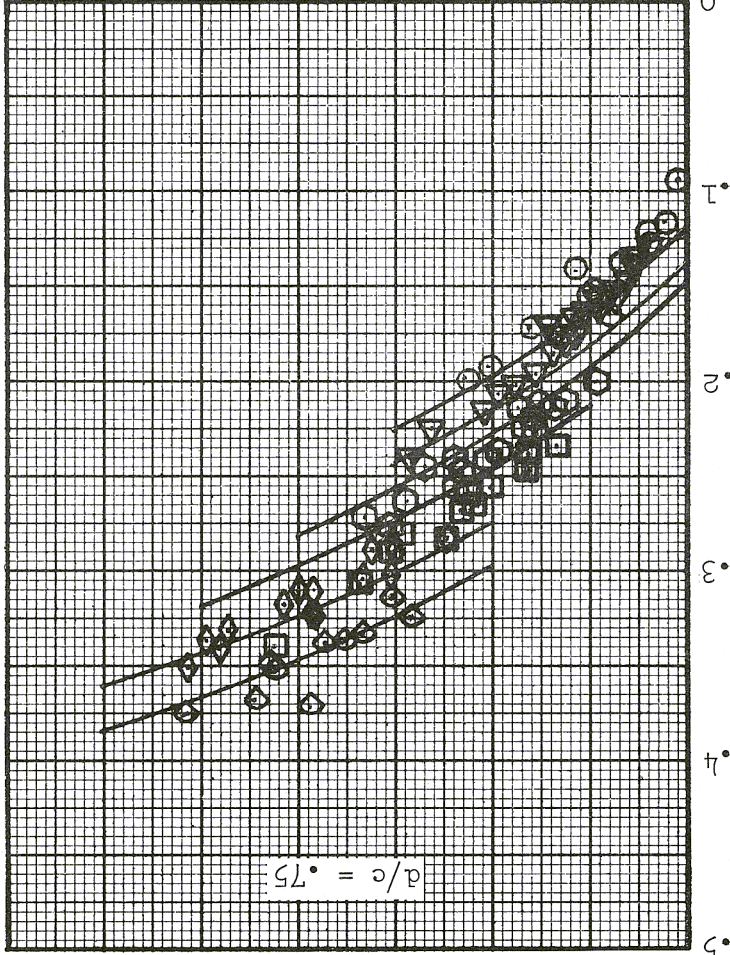
Foil Lift Coefficient – C_L

d/c = .75

FIGURE 21 DRAG CORRELATION-CAMBER EFFECT
Parent Section

A = 3 Λ = 0 λ = .5

σ = 0

Symbol	Foil No.	C_{l_i}	t/c
⬡	4	.170	.131
◯	16	.059	.071
△	17	.117	.103
☐	18	.230	.158
◇	19	.287	.180
⬡	20	.350	.203
——— Predicted			

d/c = 1.0

.350 = C_{l_i} (Typ.)
.287
.230
.170
.117
.059

d/c = 1.25

Induced Drag Coefficient - C_{D_L}

.01 .02 .03 .04 .05 .06 .07 .08

FIGURE 22 DRAG CORRELATION-TAPER RATIO EFFECT

Parent Section – C_{ℓ_i} = .170 – t/c = .131

$\Lambda = 0$ $\sigma = 0$ $A = 3.0$
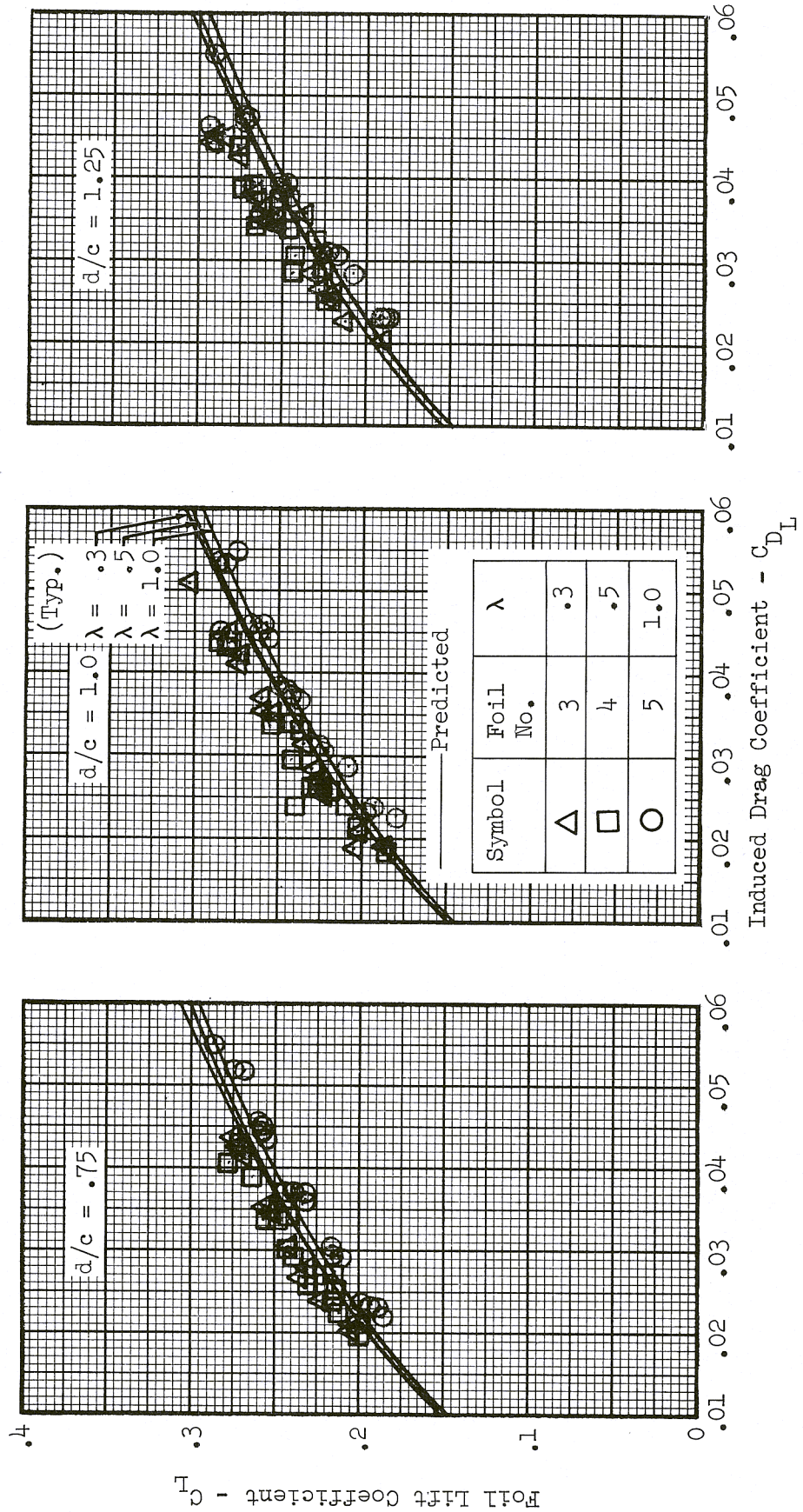
FIGURE 23 DRAG CORRELATION-SWEEP EFFECT
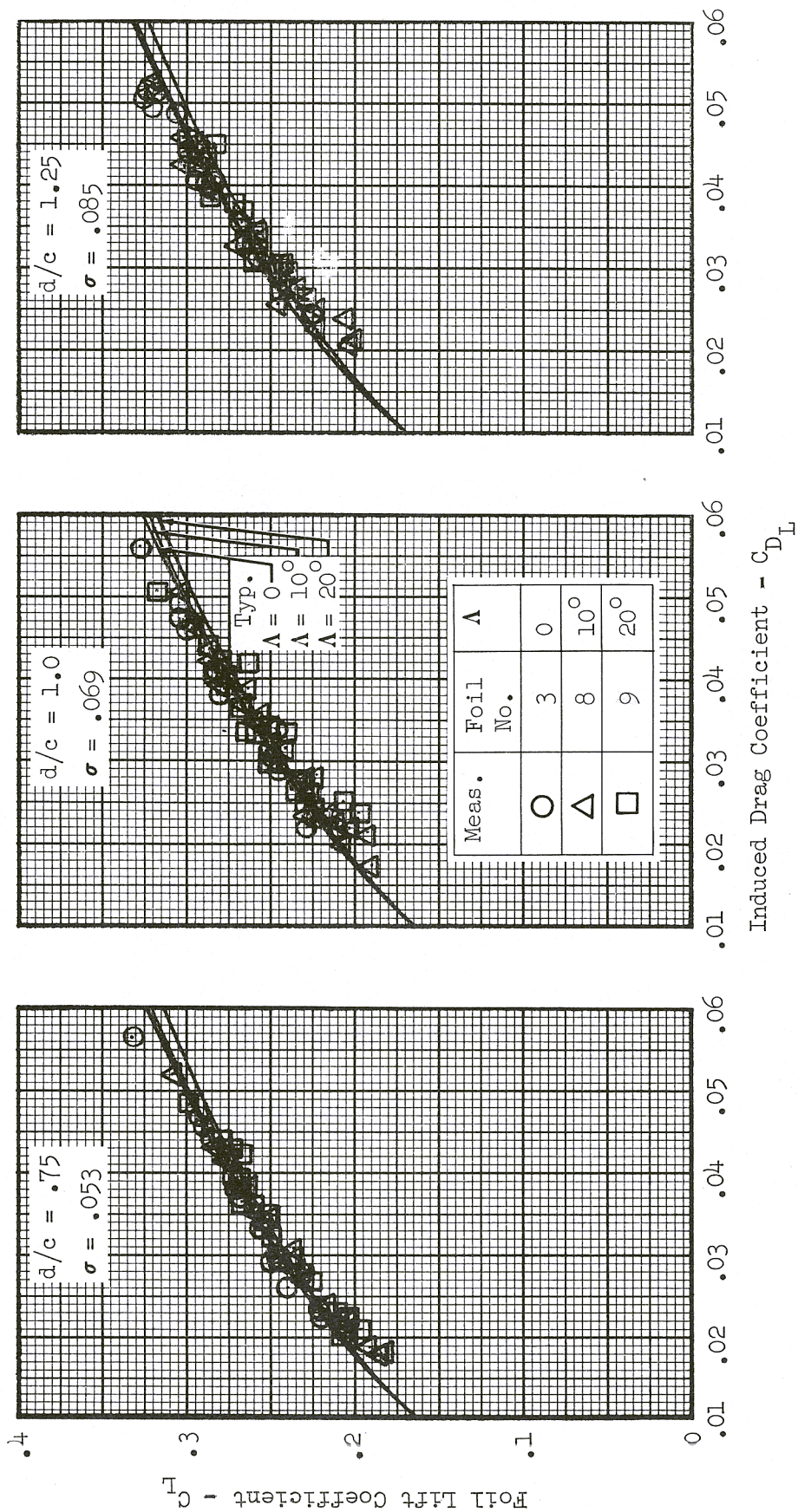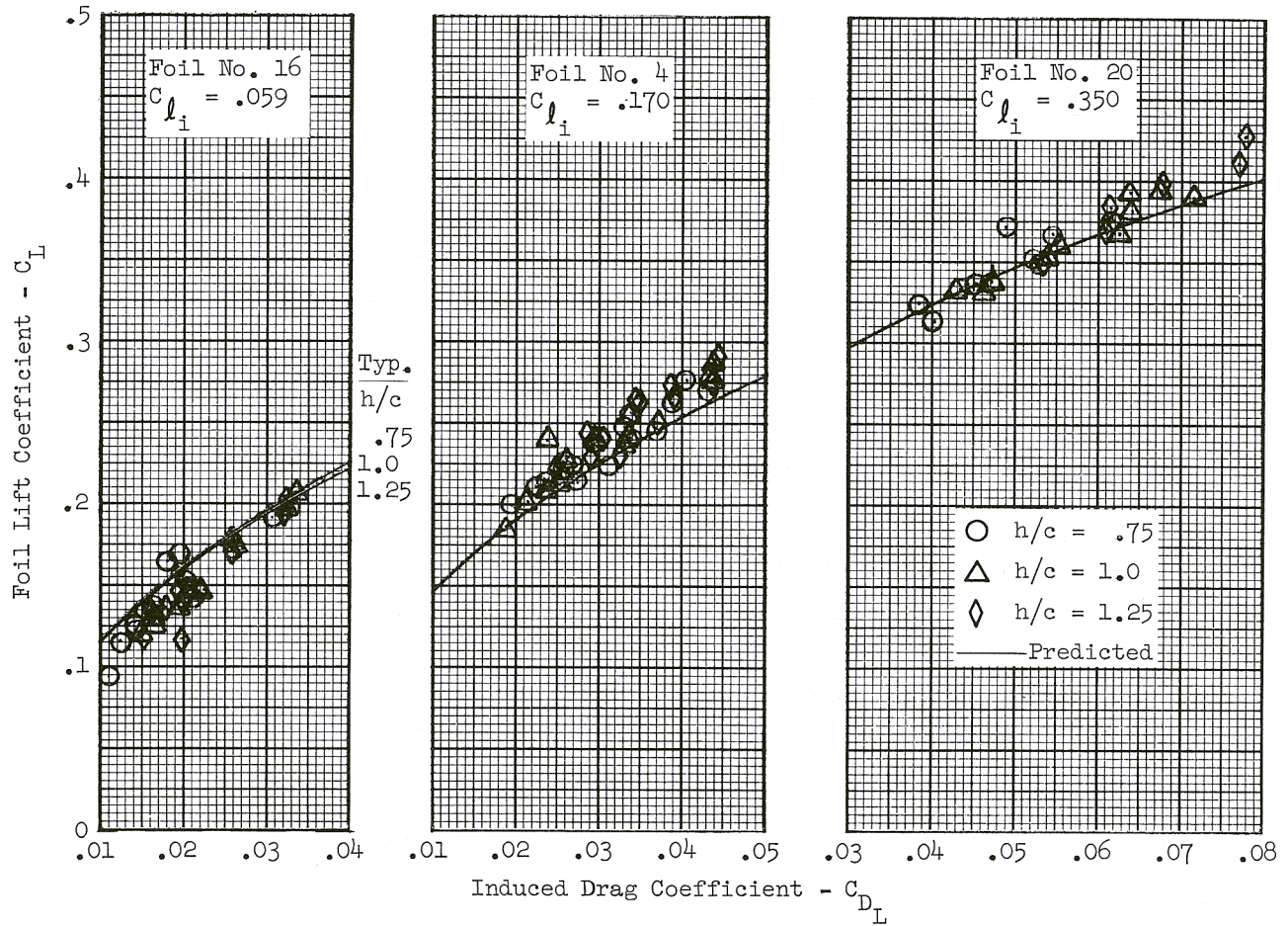
Parent Section - C_{ℓ_i} = .170 - t/c = .131

A = 3 $\qquad$ λ = .3

Meas.	Foil No.	Λ
○	3	0
△	8	10°
□	9	20°

Typ.
$\Lambda = 0$
$\Lambda = 10°$
$\Lambda = 20°$

d/c = .75
σ = .053

d/c = 1.0
σ = .069

d/c = 1.25
σ = .085

Foil Lift Coefficient - C_L

Induced Drag Coefficient - C_{D_L}

FIGURE 24   DRAG CORRELATION-SUBMERGENCE EFFECT

Parent Section

$A = 3$ $\Lambda = 0$ $\lambda = .5$

$\sigma = 0$

FIGURE 25 DRAG CORRELATION VS. α — ASPECT RATIO EFFECT
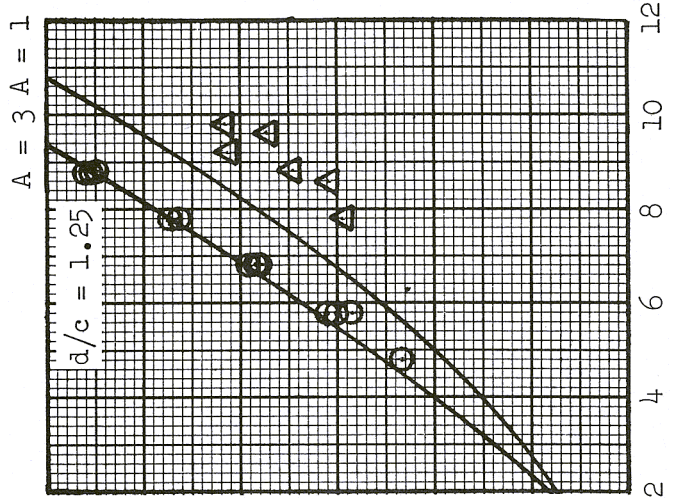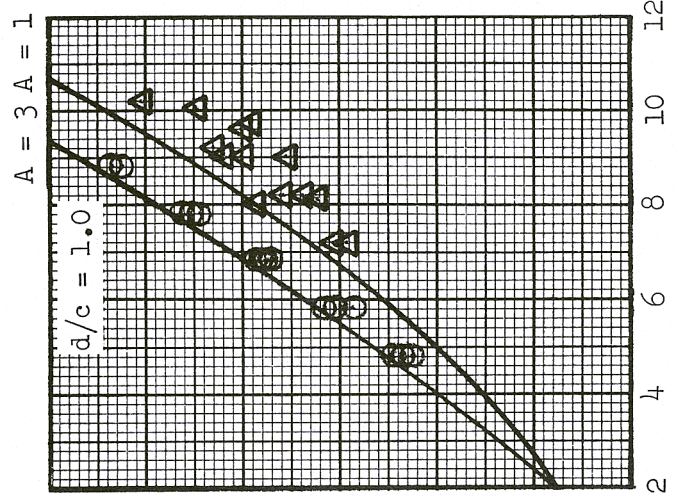Parent Section — $C\ell_i$ = .170 — t/c = .131

$\Lambda = 0$ $\sigma = 0$ $\lambda = 1.0$

Symbol	Foil No.	A
O	5	3
△	6	1

—— Predicted

Induced Drag Coefficient — C_{D_L}
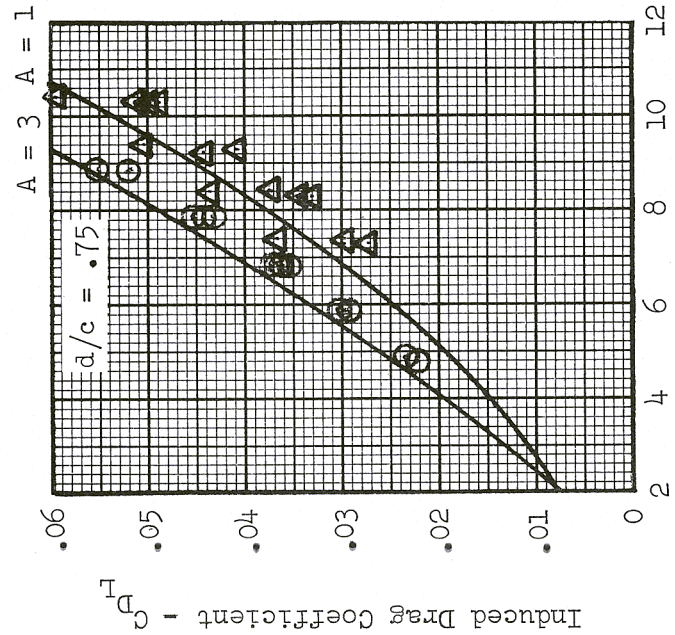
Angle of Attack, α — deg.

FIGURE 26   DRAG CORRELATION VS. α-CAMBER EFFECT
Parent Section

A = 3 $\qquad\qquad$ $\Lambda = 0$ $\qquad\qquad$ $\lambda = .5$

$\qquad\qquad\qquad\qquad$ $\sigma = 0$

Symbol	Foil No.	c_{ℓ_i}	t/c
⌓	4	.170	.131
○	16	.059	.071
△	17	.117	.103
□	18	.230	.158
◊	19	.287	.180
⬠	20	.350	.203
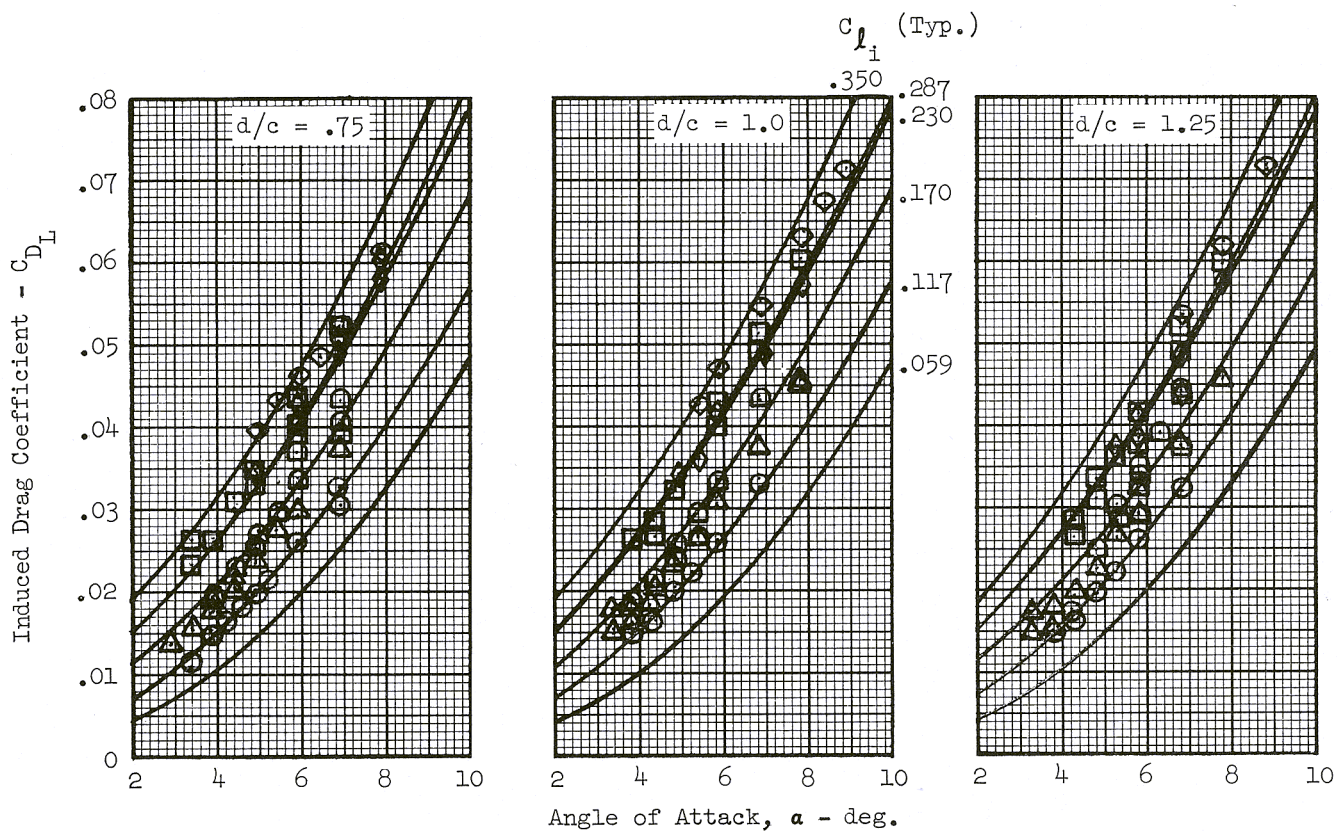
———— Predicted

FIGURE 27 DRAG CORRELATION VS. α-FOIL No. 1

Wedge – $C_{\ell_i} = 0$ – t/c = .118

A = 3	$\Lambda = 0$	$\lambda = 1.0$

——————— Predicted

Symbol	V_K	$RNx10^{-6}$
○	40	.76
△	45	.85
□	50	.95
◊	60	1.14
◯	70	1.32
⌂	80	~1.50

Induced Drag Coefficient – C_{D_L}

d/c = .75 σ = .048

d/c = 1.0 σ = .063

d/c = 1.25 σ = .078

Angle of Attack, α – deg.

Foil #1 - Wedge

.0175c

.118c

.10c

Foil #2 - Tulin

t

y_ℓ

Foil #5 - Parent

y_u

y_ℓ

Foil #10 - Flat

30%
Circular Arc

3%

Foil #16 - Cambered Parabola

y_u

y_ℓ

Strut - Parabola

y
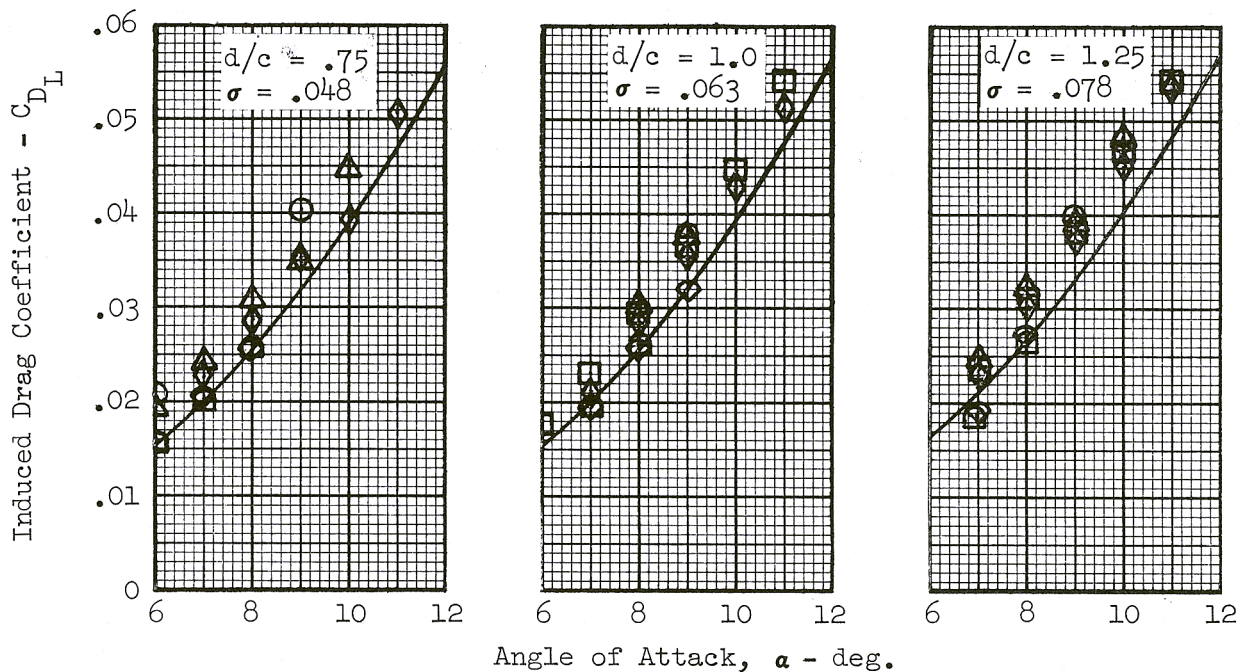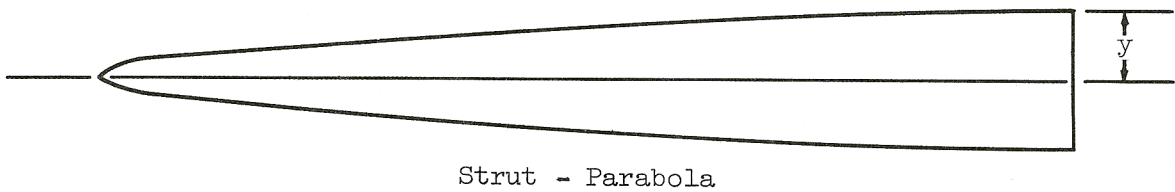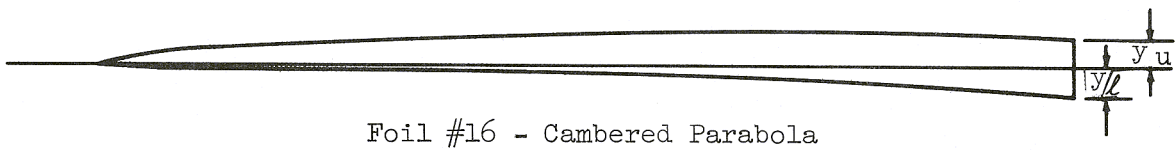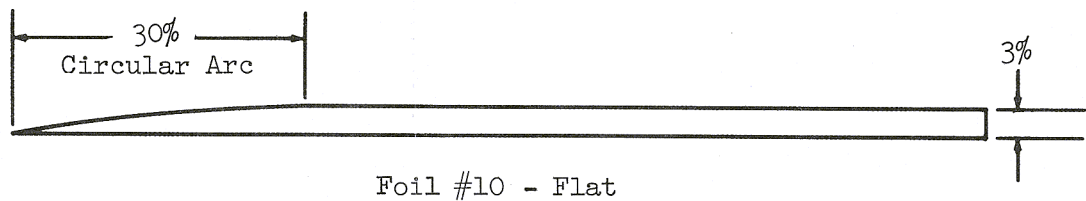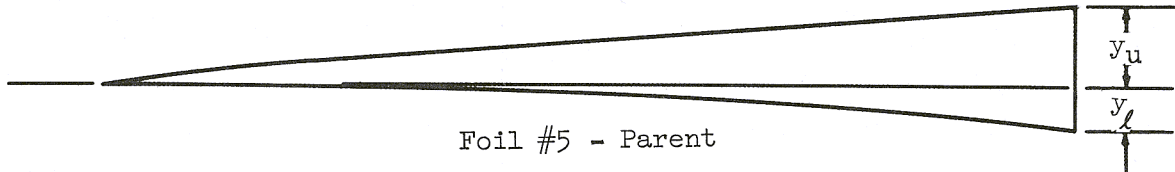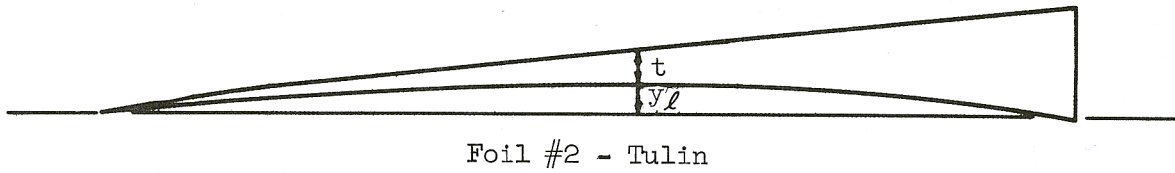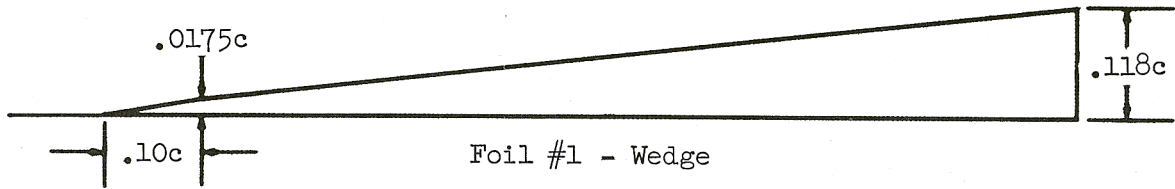
FIGURE 28
FOIL AND STRUT SECTIONS

$\frac{x}{c}$	Foil #2		Foil #5		Foil #16		Strut
	y_ℓ/c	t/c	y_ℓ/c	y_u/c	y_ℓ/c	y_u/c	y/c
0	0	0	0	0	0	0	0
.0075	.00056	.00147	–	–	.00190	.00330	.00651
.0125	.00101	.00210	–	–	.00228	.00442	.00839
.025	–	–	.0003	.0053	.00288	.00660	.01186
.050	.00441	.00520	.0004	.0084	.00355	.00987	.01680
.075	–	–	.0007	.0115	.00398	.01246	.02054
.100	.00905	.00801	.0008	.0142	.00432	.01466	.02372
.200	.01759	.01272	.0017	.0194	.00546	.02138	.03354
.300	.02436	.01815	.0028	.0334	.00671	.02615	.04108
.400	.02893	.02505	.0045	.0419	.00826	.02968	.04744
.500	.03104	.03422	.0072	.0504	.01018	.03224	.05303
.550	.03112	.03950	.0090	.0544	.01130	.03320	.05560
.600	.03053	.04557	.0110	.0582	.01253	.03395	.05810
.700	.02726	.05944	.0161	.0659	.01538	.03482	.06275
.800	.02112	.07595	.0228	.0736	.01887	.03479	.06708
.900	.01207	.09521	.0314	.0812	.02329	.03363	.07115
.950	.00642	.10591	.0365	.0849	.02608	.03240	.07310
1.000	0	.11734	.0421	.0885	.03000	.03000	.07500